0 1

AFRL-SR-BL-TR-98-

0627

REPORT DOCUMENTATION PAGE

1. AGENCY USE ONLY (Leave blank)	2. REPORT DATE	3. REPORT TYPE AND DATES COVERED
	8/26/98	Annual Technical Report

4. TITLE AND SUBTITLE

Two- and Three-Dimensional Measurements in Flames

5. FUNDING NUMBERS

PE - 61102F
PR - 2308
SA - BS
G - F49620-97-1-0096

6. AUTHOR(S)

Marshall B. Long

7. PERFORMING ORGANIZATION NAME(S) AND ADDRESS(ES)

Department of Mechanical Engineering
Yale University
P.O. Box 208284
New Haven, CT 06520-8284

8. PERFORMING ORGANIZATION REPORT NUMBER

9. SPONSORING / MONITORING AGENCY NAME(S) AND ADDRESS(ES)

AFOSR/NA
110 Duncan Avenue, Suite B115
Bolling AFB, DC 20332-0001

10. SPONSORING / MONITORING AGENCY REPORT NUMBER

11. SUPPLEMENTARY NOTES

12a. DISTRIBUTION / AVAILABILITY STATEMENT

Approved for public release; distribution is unlimited

12b. DISTRIBUTION CODE

13. ABSTRACT ***(Maximum 200 Words)***

Three-scalar measurements were made in a turbulent nonpremixed flame (Re=15000) to increase confidence in the two-scalar technique based on simultaneous imaging of Rayleigh scattering and fuel Raman scattering. Nitrogen Raman scattering was employed as an passive conserved scalar and mixture fraction was calculated by two independent approaches. These experiments showed that proper parameterization of mixture fraction-dependent terms appearing in the expression for mixture fraction can reduce deficiencies for lean values of mixture fraction and near stoichiometric. Additionally, the spatial resolution of the optical setup was characterized and determined to be sufficient for resolving scalar dissipation.

14. SUBJECT TERMS	15. NUMBER OF PAGES
Turbulent combustion, laser diagnostics, mixture fraction, scalar dissipation, nonpremixed flames	55
	16. PRICE CODE

17. SECURITY CLASSIFICATION OF REPORT	18. SECURITY CLASSIFICATION OF THIS PAGE	19. SECURITY CLASSIFICATION OF ABSTRACT	20. LIMITATION OF ABSTRACT
Unclassified	Unclassified	Unclassified	UL

TWO- AND THREE-DIMENSIONAL MEASUREMENTS IN FLAMES

AFOSR Grant No. 97-1-0096

Principle Investigator: Marshall B. Long

Yale University
Department of Mechanical Engineering and Center for Laser Diagnostics
New Haven, Connecticut 06520-8284

SUMMARY/OVERVIEW

The present research deals with improving confidence in the two-scalar mixture fraction formulation based on fuel concentration and enthalpy currently applied in turbulent nonpremixed flames. Adding a third scalar measurement to the required fuel Raman and Rayleigh scattering can reduce uncertainty around the stoichiometric contour, where fuel concentration approaches zero and the Rayleigh signal remains relatively constant. Nitrogen concentration from Raman scattering provides a simultaneous, independent, passive scalar, which has been used to modify the way functional dependences are assigned for terms appearing in the iterative calculation of mixture fraction.[1]

TECHNICAL DISCUSSION

Within the last year, a series of experiments has been focused on investigating multi-scalar measurements in turbulent nonpremixed flames. A major goal in studying such flames is to provide quantitative images of mixture fraction ξ, defined as the mass fraction of all atoms originating from the fuel stream. This allows calculation of axial and radial gradient information, and in particular the scalar dissipation χ, which controls the rate of molecular mixing. Extensive single-point measurements have been made,[2] however scalar dissipation cannot be extracted because of the lack of spatial gradient data.

One method for constructing a conserved scalar suitable for imaging experiments in reacting flows has been through the simultaneous measurement of temperature (T) and fuel concentration.[3] The conserved scalar β, is defined based on fuel mass fraction (Y_F) and enthalpy and takes the form:

$$\beta = Y_F + c_p \mathrm{T}/Q \tag{1}$$

where Q is the lower heat of combustion and c_p is the specific heat at constant pressure. This can be cast into an expression for mixture fraction:

$$\xi^{FT} \equiv \frac{\beta - \beta_{air}}{\beta_{fuel} - \beta_{air}} = \frac{Y_F + \left(c_p \mathrm{T} - c_{p,air}\mathrm{T}_{air}\right)/Q}{Y_{F,fuel} + \left(c_{p,fuel}\mathrm{T}_{fuel} - c_{p,air}\mathrm{T}_{air}\right)/Q} \tag{2}$$

This two-scalar approach, which assumes unity Lewis number and idealized one-step reaction between fuel and oxidizer, relates to the measured signals through:

$$\xi^{FT} = \frac{C_1 \sigma}{W\,Ra} Rm + \frac{C_2}{Q}\left(c_p \frac{\sigma}{Ra} - c_{p,air} T_{air} \right) \tag{3}$$

where Rm is the measured fuel Raman scattering and Ra is the Rayleigh scattering. The parameter σ, which is proportional to the Rayleigh cross section, the mixture molecular weight W, and the specific heat c_p, are dependent on the mixture fraction. Strained counterflow flame calculations provide appropriate functional forms for these parameters which are incorporated into an iterative scheme for determining ξ. The remaining constants C_1 and C_2 must be determined from calibration experiments.

This approach has been applied successfully,[4-6] however there is a need to improve the certainty in the mixture fraction calculation around the stoichiometric contour. At this location, the fuel concentration approaches zero and the Rayleigh signal remains nearly constant. The present work has examined Raman scattering from nitrogen as a third scalar measurement to improve confidence in the two-scalar mixture fraction calculation.

In order for the N_2 Raman channel to provide an independent conserved scalar with sufficient signal variation between regions of pure air and pure fuel, experiments were performed in which the fuel stream contained no nitrogen. Assuming no significant nitrogen consumption occurs during reaction, we can write the conserved scalar in terms of nitrogen mass fraction:

$$\beta^{N_2} \equiv Y_{N_2} \tag{4}$$

with the mixture fraction:

$$\xi^{N_2} = 1 - \frac{Y_{N_2}}{Y_{N_2,\mathrm{air}}} = 1 - \frac{C_3\,\sigma}{W\,Ra} Rm_{N_2} \tag{5}$$

where Rm_{N_2} is the nitrogen Raman signal, and C_3 is an additional calibration constant. This formulation requires measurement of the temperature and nitrogen concentration, and thus, represents an additional two-scalar approach. The fuel mixture (25% methane, 59% argon, and 16% oxygen by volume), has a stoichiometric mixture fraction ξ_s=0.41, putting the reaction zone well inside the shear layer.

Simultaneous planar Rayleigh, fuel Raman, and nitrogen Raman images have been collected in experiments using three cameras and a single laser. Figure 1 shows the experimental facility, which is described in detail elsewhere and summarized here.[1] A flashlamp-pumped dye laser is employed in an intracavity configuration to generate single-shot energies up to 4.7 J at 532 nm. The beam is focused into a sheet over a 6.1 mm diameter piloted burner. Scattered light is collected on both sides of the flame by low $f\#$ camera lenses oriented perpendicular to the laser sheet. The Rayleigh scattering and fuel Raman scattering are collected along the same optical path and divided with a 50/50 pellicle beam splitter, while the weaker nitrogen Raman scattering is collected along the opposite optical path. Image intensifiers are lens-coupled to liquid-cooled CCD cameras and isolated with appropriate interference filters.

In the past, the imaging resolution of the optical setup has been characterized in terms of the volume associated with each pixel. For the present work, the pixel volume is 49×49×500 μm^3, where the largest value corresponds to the laser sheet thickness, and the remaining dimensions describe the area imaged onto a single pixel. The actual spatial resolution is a more complex function of the optical layout, including alignment, lenses, filters, image intensifiers, and camera pixel size. In order to better quantify the spatial resolution for this configuration, simultaneous images have been taken of a uniformly illuminated 25 μm wire located at the focal plane. Individual camera resolutions are based upon the resulting full-width half-maximum (FWHM) intensity of the wire image from each camera following scaling, translation, rotation, and cropping. The spatial resolution is 170 μm on the Rayleigh camera, 140 μm on the nitrogen Raman camera, and 275 μm on the fuel Raman camera. Translating the wire normal to the plane of the laser sheet within the beam thickness (± 250 μm from the focal plane) has minimal effect (<10%) on the individual camera resolutions.

Because this is a multi-camera experiment and the cameras are located along different optical trains, there remains the issue of how well the images correlate on a pixel-by-pixel basis. Cross-camera spatial resolutions here are defined based upon adding combinations of matched images from each camera, and measuring the resultant full-width half-maximum of the wire. With optimal matching, the on-axis spatial resolution is 280 μm, about equal to the largest single camera resolution. Factors such as distortion may cause degradation away from the optical axis to a maximum measured 400 μm. Using the $1/e^2$ intensity point rather than the FWHM for determining spatial resolution increases the reported values by ~75%.

Estimates of the Kolmogorov scale (κ) on the centerline for a diluted methane flame (3/1 air/methane by volume) give a value of κ=95 μm at Re=20,600.[4] Using this as an approximate value for the turbulent flame in this work, the resolutions reported here are in the range 2-4κ. A study of an isothermal jet performed by Namazian, et al. reports that a spatial resolution of 5κ should be sufficient for capturing 60% of the scalar dissipation spectrum.[7] In flames, where heat release is expected to increase length scales, a resolution of 5κ should be sufficient to record most of the scalar dissipation.[4]

Figure 2 shows line plots of mixture fraction from a laminar flame (Re=1600) at a location 15 nozzle diameters downstream (D=6.1 mm). Two curves are shown for ξ^{FT}, which differ in the parameterization of the mixture fraction dependent terms appearing in Eqn. 3 (i.e. σ, W, c_p). The curve marked "No lean correction" uses flame calculation terms parameterized by "actual" mixture fraction determined from the Bilger formula.[8]

Figure 3 shows that this approach incorporates a departure of ξ^{FT} from the more rigorous formulation, as indicated by strained laminar flame calculations (strain rate=100 s^{-1}). Deviation from one-step chemistry (i.e. loss of parent fuel to intermediate species) is compensated in the curve marked ξ_{cor}^{FT} by using a weighting term involving reactivity.[9] The curve for ξ^{N_2} exhibits little deviation from the actual mixture fraction. By assigning functional dependences based on the predicted ξ^{FT} from flame calculations, the ξ^{FT} curve shown in Fig. 2 is obtained showing improved agreement with ξ^{N_2}. The flame computations are insensitive to variations in the strain rate

over the range 10-200 s^{-1}, which is expected to be representative of the scalar dissipation values measured in the turbulent flame, based on existing data in similar flames.[8,10]

Applying this technique to single-pulse imaging in turbulent nonpremixed flames provides similar results, although the N_2 Raman signal is affected by noise, especially in regions of high mixture fraction where there is little nitrogen. Figure 4 shows images taken 25*D* downstream from a *Re*=15,000 turbulent flame; the Raman images have been contour smoothed.[11] Qualitatively, the scalar dissipation fields, χ (defined as $\chi \equiv 2\mathcal{D}\nabla\xi\cdot\nabla\xi$, where $\mathcal{D}$ is the diffusivity), appear similar, revealing the same main structural features, with significant scalar dissipation apparent along the edge of the main jet. The position of the stoichiometric mixture fraction contour is highlighted (black lines) in these images.

In summary, recent experiments measuring nitrogen-temperature mixture fraction have served as a guide for correcting the fuel-temperature mixture fraction for values around and lean of stoichiometric. It has been shown that parameterizing specific heat, molecular weight, and Rayleigh cross section as a function of ξ^{FT} predicted from counterflow flame calculations, rather than the actual mixture fraction, improves the performance of this two-scalar approach. Under turbulent conditions (*Re*=15,000), the two approaches reveal differences close to the centerline, most likely a result of noise limitations of the nitrogen Raman signal. This work increases confidence in employing ξ^{FT} for mixture fraction determination, which remains the most attractive approach because of its superior signal-to-noise characteristics. Further details of the results are documented in the paper accepted to the Twenty-Seventh Symposium on Combustion, which will be published later this year.[1]

REFERENCES

1. Fielding, J., Schaffer, A.M., Long, M.B.,*Twenty-Seventh Symposium (International) on Combustion*, (in press) The Combustion Institute, Pittsburgh, PA, 1998.
2. Masri, A.R., Dibble, R.W., and Barlow, R.S., *Prog. Energy Combust. Sci.* 22:307-362 (1996).
3. Stårner, S.H., Bilger, R.W., Dibble, R.W., and Barlow, R.S., *Combust. Sci. and Tech.* 86:223-236 (1992).
4. Stårner, S.H., Bilger, R.W., Lyons, K.M., Frank, J.H., and Long, M.B., *Combust. Flame.* 99:347-354 (1994).
5. Frank, J.H., Lyons, K.M., Marran, D.F., Long, M.B., Stårner, S.H., and Bilger, R.W., *Twenty-Fifth Symposium (International) on Combustion*, The Combustion Institute, Pittsburgh, PA, 1994, pp. 1159-1166.
6. Long, M.B., Frank, J.H., Lyons, K.M., Marran, D.F., and Stårner, S.H., *Ber. Bunsenges. Phys. Chem.*, 97:1555-1559 (1993).
7. Namazian, M., Schefer, R.W., and Kelly, J., *Comb. and Flame*, 74:147-160 (1988).
8. Bilger, R.W., Stårner, S.H., and Kee, R.J., *Comb. and Flame*, 80:135-149 (1990).
9. Stårner, S.H., Bilger, R.W., Long, M.B., Frank, J.H., and Marran, D.F., *Combust. Sci. Tech.* 129:141-163 (1997).
10. Kelman, J.B., and Masri, A.R., *Combust. Sci. and Tech.* 129:17-55 (1997).
11. Stårner, S.H., Bilger, R.W., and Long, M.B., *Combust. Sci. and Tech.* 107:195-203 (1995).

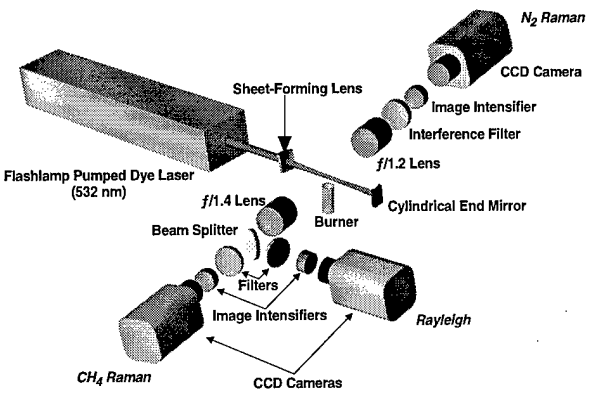

Figure 1. Schematic of the three-scalar intracavity turbulent flame imaging experiment.

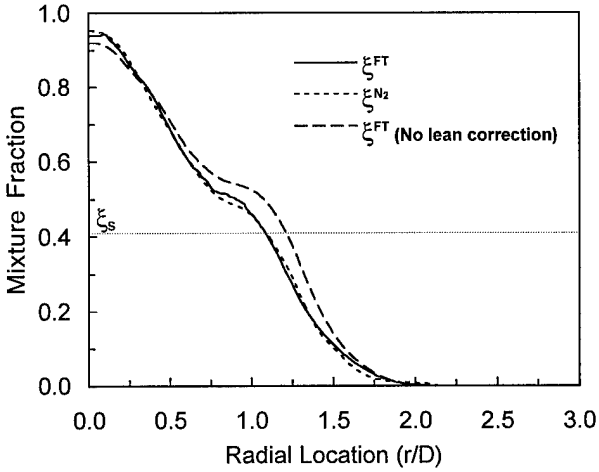

Figure 2. Radial variation of mixture fraction calculated from fuel-temperature (solid line) and nitrogen-temperature (short dashes) two-scalar approaches 15*D* downstream in a laminar flame (Re=1600). ξ^{FT} overpredicts the fuel-temperature mixture fraction in regions around and lean of stoichiometric (long dashes).

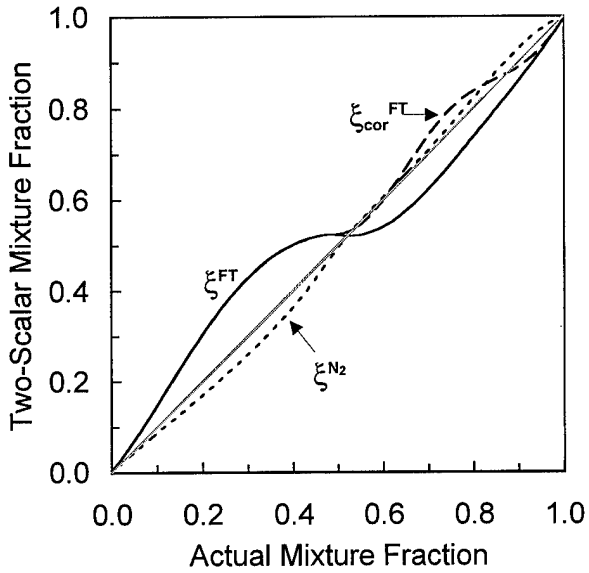

Figure 3. Mixture fraction calculated from strained laminar flame calculations (100 s^{-1}) using the fuel-temperature (solid line) and nitrogen-temperature (short dashes) two-scalar approaches plotted against mixture fraction calculated using the formula proposed by Bilger [7]. The effect of fuel correction on ξ^{FT} is shown (long dashes).

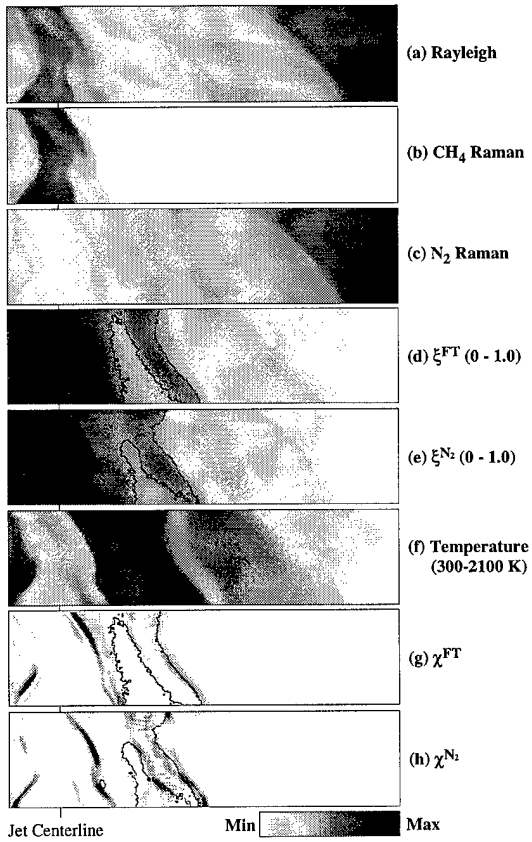

Figure 4. Instantaneous (a) Rayleigh, (b) CH_4 Raman, (c) N_2 Raman images of the turbulent flame taken 25 jet diameters (*D*=6.1 mm) downstream. Also shown are the computed mixture fraction images (d) ξ^{FT}, (e) ξ^{N_2}, (f) temperature, and scalar dissipation images (g) χ^{FT}, and (h) χ^{N_2}. Each image size is $4.3D \times 1D$.

ATTACHMENTS

1. PIADC Form

2. S.H. Stårner, R.W. Bilger, M.B. Long, J.H. Frank, and D.F. Marran, "Scalar Dissipation Measurements in Turbulent Jet Diffusion Flames of Air Diluted Methane," *Combust. Sci. Tech.* **129**, 141 (1997).

3. J. Fielding, A.M. Schaffer, and M.B. Long, "Three-Scalar Imaging in Turbulent Nonpremixed Flames of Methane," *Twenty-Seventh Symposium (International) on Combustion*, The Combustion Institute, in press (1998).

Principal Investigator Annual Data Collection (PIADC) Survey Form

NOTE: If there is insufficient space on this survey to meet your data submissions, please submit additional data in the same format as identified below.

PI DATA

Name (Last, First, MI): Long, Marshall B.

Institution: Yale University

Contract/Grant No: F49620-97-1-00096

AFOSR USE ONLY
Project/Subarea
_____/____

NX _____

FY _____

NUMBER OF CONTRACT/GRANT CO-INVESTIGATORS

Faculty 1 Post Doctorates 0 Graduate Students 2 Other 0

PUBLICATIONS RELATED TO AFOREMENTIONED CONTRACT/GRANT

NOTE: List names in the following format: Last Name, First Name, MI

Include: Articles in peer reviewed publications, journals, book chapters, and editorships of books.

Do Not Include: Unreviewed proceedings and reports, abstracts, "Scientific American" type articles, or articles that are not primary reports of new data and articles submitted or accepted for publication, but with a publication date outside the stated time frame

Name of Journal, Book, etc: Combustion Science and Technology

Title of Article: Scalar Dissipation Measurements in Turbulent Jet Diffusion Flames of Air Diluted Methane and Hydrogen

Author(s): S.H. Stårner, R.W. Bilger, M.B. Long, J.H. Frank, and D.F. Marran

Publisher (if applicable): Gordon and Breach

Volume: 129 Page(s): 141-163 Month Published: _____ Year Published: 1997

Name of Journal, Book, etc: Proceedings of the Twenty-Seventh Symposium on Combustion

Title of Article: Three-Scalar Imaging in Turbulent Non-Premixed Flames of Methane

Author(s): J. Fielding, A.M. Schaffer, and M.B. Long

Publisher (if applicable): The Combustion Institute

Volume _____ Page(s) _____ Month Published _____ Year Published: 1998

THREE-SCALAR IMAGING IN TURBULENT NONPREMIXED FLAMES OF METHANE

JOSEPH FIELDING, ANDREW M. SCHAFFER, AND MARSHALL B. LONG[†]

Yale University

Department of Mechanical Engineering and Center for Laser Diagnostics

New Haven, Connecticut 06520-8284, USA

27th International Symposium on Combustion

University of Colorado, Boulder, CO

August 2-7, 1998

[†] Corresponding Author:

Professor Marshall B. Long
Department of Mechanical Engineering
Yale University
New Haven, CT 06520-8284, USA
Phone: (203) 432-4229
Fax: (203) 432-6775
email: mblong@cld3.eng.yale.edu

Abstract

Raman scattering from nitrogen in laminar (*Re*=1600) and turbulent (*Re*=15,000) nonpremixed flames of diluted methane has been investigated as a means of complementing the two-scalar mixture fraction computation based on measurements of fuel mass fraction and temperature (ξ^{FT}). Using a diluent consisting of argon and oxygen with an overall volumetric dilution ratio of 3/1 (diluent/fuel) allows sufficient variation in the measured nitrogen concentration for its use as a passive scalar. The present experimental setup requires only a single laser (532 nm) in a high-power intracavity configuration. Mixture fraction profiles calculated using independent fuel-temperature and nitrogen-temperature two-scalar approaches show excellent agreement in the laminar flame. For the turbulent flame, a 100 single-shot average of mixture fraction shows reasonable agreement between the two approaches. Discrepancies are most evident in single-shot images in regions of large mixture fraction ($\xi>\xi_s$) where the nitrogen Raman signal is noise-dominated. The location of the stoichiometric contour is consistently determined by both two-scalar approaches. A simple modification of the functional dependence for parameters appearing in the fuel-temperature mixture fraction formulation is shown to correct deficiencies in the approach predicted by laminar flame calculations, most notably for values of ξ^{FT} around stoichiometric and into lean regimes.

Introduction

Planar imaging of turbulent flames using laser diagnostic techniques such as Lorenz-Mie [1], Rayleigh [2], laser-induced fluorescence [3], and Raman scattering [4], have long been directed towards improved characterization of the flow structures and flame front location. One major goal in studying turbulent flames is to provide quantitative images of mixture fraction ξ, defined as the mass fraction of all atoms originating from the fuel stream. This allows calculation of axial and radial gradient information, and in particular the scalar dissipation χ, which controls the rate of molecular mixing. Experimental data are essential for modelers to construct joint probability density functions conditional on these parameters. Extensive single-point measurements have been made [5], however scalar dissipation cannot be extracted because of the lack of spatial gradient data. Line-Raman measurements [6,7] are less restrictive, allowing the computation of one-dimensional scalar dissipation.

One method for constructing a conserved scalar suitable for reacting flows has been through the simultaneous measurement of temperature (T) and fuel concentration [8]. The conserved scalar β, is defined based on fuel mass fraction (Y_F) and enthalpy and takes the form:

$$\beta = Y_F + c_p \mathrm{T}/Q$$

where Q is the lower heat of combustion and c_p is the specific heat at constant pressure. This can be cast into an expression for mixture fraction:

$$\xi^{FT} \equiv \frac{\beta - \beta_{air}}{\beta_{fuel} - \beta_{air}} = \frac{Y_F + c_p(\mathrm{T} - \mathrm{T}_{air})/Q}{Y_{F,fuel} + c_p(\mathrm{T}_{fuel} - \mathrm{T}_{air})/Q}$$

This two-scalar approach, which assumes unity Lewis number and idealized one-step reaction between fuel and oxidizer, relates to the measured signals through:

$$\xi^{FT} = \frac{\mathrm{C}_1 \sigma}{W\,Ra} Rm + \mathrm{C}_2 \frac{c_p}{Q}\left(\frac{\sigma}{Ra} - \mathrm{T}_{air}\right)$$

where *Rm* is the measured fuel Raman scattering and *Ra* is the Rayleigh scattering. The parameter σ, which is proportional to the Rayleigh cross section, the mixture molecular weight W, and the specific heat c_p, are dependent on the mixture fraction. Strained counterflow flame calculations provide appropriate functional forms for these parameters which are incorporated into an iterative scheme for determining ξ. The remaining constants C_1 and C_2 must be determined from calibration experiments.

This approach has been applied successfully [3, 9-14], however there is a need to improve the certainty in the mixture fraction calculation around the stoichiometric contour. At this location, the fuel concentration approaches zero and the Rayleigh signal remains nearly constant. The acquisition of an appropriate third scalar with continuously varying signal could improve confidence in the two-scalar mixture fraction calculation in this regime by providing independent quantitative confirmation of the measurements. The present work examines Raman scattering from nitrogen as a third scalar measurement in turbulent nonpremixed flames.

In this paper, simultaneous planar Rayleigh, fuel Raman, and nitrogen Raman images have been collected in experiments using three cameras and a single laser. Current detector technology combined with high-energy (~5 J/pulse) laser configurations makes Ramanography feasible for molecules such as nitrogen, despite its small scattering cross-section [15]. In order for the N_2 Raman channel to provide an independent passive conserved scalar with sufficient signal variation between regions of pure air and pure fuel, experiments were performed in which the fuel stream contained no nitrogen. Assuming no significant nitrogen consumption occurs during reaction, we can write the conserved scalar in terms of nitrogen mass fraction:

$$\beta^{N_2} \equiv Y_{N_2}$$

with the mixture fraction:

$$\xi^{N_2} = 1 - \frac{Y_{N_2}}{Y_{N_2,\text{air}}} = 1 - \frac{C_3\,\sigma}{W\,Ra} Rm_{N_2}$$

where Rm_{N_2} is the nitrogen Raman signal, and C_3 is an additional calibration constant. This formulation requires measurement of the temperature and nitrogen concentration, and thus, represents an additional two-scalar approach.

Experiment

The experimental facility used in the present work to measure Rayleigh, fuel Raman, and nitrogen Raman scattering is shown schematically in Fig. 1. A single flashlamp-pumped dye laser (Candela LFDL-20; Pyrromethene 546 dye, $2.0\times10^{-5}M$ in methanol) is employed in an intracavity configuration to generate single-shot energies up to 4.7 J at 532 nm. The beam is focused into a sheet by a 30-cm focal-length cylindrical lens, and an 8 mm wide slit inserted into the cavity provides a beam waist of 500 μm. Beam waist measurements are performed by imaging the laser sheet from above using Lorenz-Mie scattering from NaCl particles seeded into air with a nebulizer (TSI Model 9306).

Scattered light is collected on both sides of the flame by low $f\#$ camera lenses oriented perpendicular to the laser sheet. The Rayleigh scattering and fuel Raman scattering are collected along the same optical path and divided with a 50/50 pellicle beam splitter, while the weaker nitrogen Raman scattering is collected along the opposite optical path. Image intensifiers are lens-coupled to liquid-cooled CCD cameras and isolated with appropriate 10 nm bandwidth interference filters. The filters and cameras used are: 532 nm (center wavelength) for the Rayleigh scattering (Photometrics Star1 CCD), 630 nm for the Stokes-shifted Raman scattering from methane (Photometrics CH250), and 610 nm for nitrogen Raman scattering (Princeton Instruments TE/CCD-512). The image intensifiers are gated for the same 2 μs period to bracket the laser pulse and minimize background interferences from flame luminosity. The experiment is controlled from a single computer which handles the subsequent image transfer and storage. Raw images are corrected for background and throughput as described in Ref. 16.

In the past, the imaging resolution of the optical setup has been characterized in terms of the volume associated with each pixel. For the present work, the pixel volume is 49×49×500 μm^3, where the largest value corresponds to the laser sheet thickness, and the remaining dimensions describe the area imaged onto a single pixel. The actual spatial resolution is a more complex function of the optical layout, including alignment, lenses, filters, image intensifiers, and camera pixel size. In order to better quantify the spatial resolution for this configuration, simultaneous images have been taken of a uniformly illuminated 25 μm wire located at the focal plane. Individual camera resolutions are based upon the resulting full-width half-maximum (FWHM) intensity of the wire image from each camera following scaling, translation, rotation, and cropping. The spatial resolution is 170 μm on the Rayleigh camera, 140 μm on the nitrogen Raman camera, and 275 μm on the fuel Raman camera. Translating the wire normal to the plane of the laser sheet within the beam thickness (± 250 μm from the focal plane) has minimal effect (<10%) on the individual camera resolutions.

Because this is a multi-camera experiment and the cameras are located along different optical trains, there remains the issue of how well the images correlate on a pixel-by-pixel basis. Cross-camera spatial resolutions here are defined based upon adding combinations of matched images from each camera, and measuring the resultant full-width half-maximum of the wire. With optimal matching, the on-axis spatial resolution is 280 μm, about equal to the largest single camera resolution. Factors such as distortion may cause degradation away from the optical axis to a maximum measured 400 μm. Using the $1/e^2$ intensity point rather than the FWHM for determining spatial resolution increases the reported values by ~75%.

Estimates of the Kolmogorov scale (κ) on the centerline for a diluted methane flame (3/1 air/methane by volume) give a value of κ=95 μm at Re=20,600 [9]. Using this as an approximate value for the turbulent flame in this work, the resolutions reported here are in the range 2-4κ. A study of an isothermal jet performed by Namazian, et al. [17] reports that a spatial resolution of 5κ

should be sufficient for capturing 60% of the scalar dissipation spectrum. In flames, where heat release is expected to increase length scales, a resolution of 5κ should be sufficient to record most of the scalar dissipation [9].

The burner consists of a 6.1 mm diameter nozzle surrounded by a 14 mm pilot flame region, which prevents blowoff of the turbulent flames and allows examination of a large range of Reynolds numbers. The premixed pilot flame is fueled by stoichiometric acetylene/hydrogen/air in proportions such that the mixture carbon/hydrogen ratio matches that of the main jet, which allows the flame to be modeled as a two-stream mixing problem [18]. A filtered ambient air coflow (~7 m/s) prevents entrainment of dust into the flame that would interfere with the Rayleigh measurement. The fuel used in this work is methane mixed with argon and oxygen to provide a 3/1 dilution ratio by volume and a diluent oxygen content to match that of air. For this fuel composition, the stoichiometric mixture fraction is $\xi_s = 0.41$ which puts the reaction zone well inside the shear layer.

Dilution suppresses much of the soot and formation of soot precursors that can affect the nitrogen Raman signal [19]. In the laminar flame, C_2 fluorescence contributes about 15% to the N_2 Raman signal on the rich side of the flame front when isolated with the 10 nm bandwidth interference filter. Using a narrower 3 nm bandwidth filter centered at a wavelength of 607.3 nm virtually eliminates this interference at a loss of half of the Raman signal. The 3 nm filter is used for the laminar flame results presented in the next section. The broader 10 nm bandwidth filter is used for the turbulent flame imaging to provide maximum SNR, as the interference is expected to be less significant than under laminar flame conditions.

The N_2 Raman images are corrected for temperature dependence of the scattering cross section and the overlap of the Raman spectral profile with the bandpass of the interference filter. Simple convolution of the temperature-dependent Raman spectrum (computed using the Raman code developed by Hassel [20]) with the zero-degree-incidence filter profile gives a correction factor that does not adequately predict the signal variation with temperature. This effect is a consequence of

the placement of the interference filter relative to the collection lens. A geometric analysis reveals that off-axis rays entering the filter create a significant shift in the effective spectral profile towards shorter wavelengths. A series of calibration experiments, in conjunction with the geometric analysis, is used to provide the temperature correction. The magnitude of the N_2 Raman correction is as high as 50% at the peak flame temperatures (T_{ad}≈2200 K) for the 10 nm bandwidth interference filter. This temperature dependence is partly beneficial in that ample N_2 Raman signal is available even at higher temperatures. A similar analysis applied to the methane Raman signal indicates no off-axis ray correction is necessary.

Calibration images are taken before and after each experimental sequence in flows of known uniform concentration (helium, methane, and air). Additionally, a series of measurements performed in a non-reacting jet of fuel issuing into ambient air (T_1=T_2=298 K) confirms the precision of the temperature images, with maximum fluctuations about the mean of ± 10 K and a signal-noise ratio (SNR) of 70.

Results and Discussion

Images have been obtained from a laminar flame (*Re*=1600) taken 15 nozzle diameters (*D*) downstream of the jet exit, and from a turbulent flame (*Re*=15,000) at a distance 25*D* downstream. Data from the laminar flame represent a 50-shot average, which gives a Rayleigh SNR of 250 in the ambient air region. Fuel Raman SNR is 30 in the fuel core, and the nitrogen Raman has SNR values of 20 in the ambient air. A contour smoothing technique [21] has been applied to both Raman channels, which improves the fuel Raman SNR by a factor of 2 and the nitrogen Raman by more than a factor of 10.

Figure 2 shows the scattered signals along a line (one pixel height) as a function of the normalized radius. The flattening of the N_2 Raman profile around r/*D* = 0.75 is attributable to the temperature sensitivity of the signal; increased spectral overlap with the interference filter occurs at higher temperatures for this experimental setup. Figure 3 shows mixture fraction as a function of

radius in the laminar flame computed using fuel-temperature (ξ^{FT}) and nitrogen-temperature (ξ^{N_2}) two-scalar approaches. There is good agreement between the two profiles, and both predict a centerline mixture fraction just over $\xi \approx 0.9$, and the radial location of the stoichiometric contour coincides.

Counterflow flame calculations (strain rate=100 s^{-1}) of this system demonstrate the departure of the two-scalar formulation from the "actual" mixture fraction (Fig. 4) calculated using the Bilger formula [22]:

$$\xi \equiv \frac{2Z_C/W_C + \frac{1}{2}Z_H/W_H + \left(Z_{O,air} - Z_O\right)/W_O}{2Z_{C,fuel}/W_C + \frac{1}{2}Z_{H,fuel}/W_H + \left(Z_{O,air} - Z_{O,fuel}\right)/W_O}$$

where Z_i and W_i are the atomic mass fractions and weights, respectively, for carbon (C), hydrogen (H), and oxygen (O). Deviation from one-step chemistry (i.e. loss of parent fuel to intermediate species) is compensated in calculating fuel concentration by the expression $Rm_F = Rm_{F,0}$ $(1 + C_F \Phi^2)$, where $Rm_{F,0}$ is the uncompensated value, and the reactivity is defined as $\Phi = (T - T_{ambient})/(T_{ad} - T_{ambient})$ [12]. C_F is a weighting coefficient ($C_F = 0.8$) and, as illustrated in the figure by the curve marked ξ_{cor}^{FT}, corrects on the rich side of stoichiometric. The slight plateau in mixture fraction shown in Figure 3 coincides with the deviation occurring near $\xi^{FT}=0.5$ in Fig. 4, and spatially coincides with the peak temperature. It is also predicted from the flame calculations that the mixture fraction based upon nitrogen mass fraction should exhibit little deviation from ξ. To correct ξ^{FT} on the lean side, $c_p(\xi)$, $\sigma(\xi)$, and $W(\xi)$ are described as functions of the predicted two-scalar mixture fraction ξ^{FT}, rather than the actual mixture fraction from the flame calculations. The latter approach gives the third curve in Fig. 3 (denoted F-T no lean correction), which overpredicts the mixture fraction -- in agreement with the trends indicated in Fig. 4. Without this simple modification, the location of the stoichiometric contour is in error by $0.1D$ towards the lean side.

The temperature correction of the N_2 Raman signal causes a minor dependence of ξ^{N_2} on the value of ξ^{FT} because the latter is used to adjust the Rayleigh cross section parameter, $\sigma(\xi)$. This effect is small, however, and the magnitude of the temperature correction is reduced by 20% in the turbulent flame measurement because of the larger bandwidth interference filter. The flame computations are insensitive to variations in the strain rate over the range 10-200 s^{-1}, which is expected to be representative of the scalar dissipation values measured in the turbulent flame, based on existing data in similar flames [12, 14, 21].

For the turbulent flame, 100 instantaneous images were processed and then averaged. Figure 5 shows the Rayleigh and Raman profiles. Comparison of the computed mixture fractions in Fig. 6 shows good agreement between the two approaches, and the location of the stoichiometric contour again coincides. For values $\xi>\xi_S$, there is some discrepancy between the profiles of ξ^{FT} and ξ^{N_2}, and peak centerline mixture fractions are $\xi^{FT}_{r=0}=0.75$ versus $\xi^{N_2}_{r=0}=0.80$. These discrepancies may reflect the limitations in ξ^{FT} caused by the deviation from the actual mixture fraction indicated in Fig. 4; however, the maximum discrepancy between the two profiles has a width of only $0.2D$. Again, failure to parameterize the variables in the two-scalar mixture fraction with respect to predicted ξ^{FT} would have caused a larger discrepancy in the mixture fraction obtained with the different two-scalar techniques.

In order to examine the performance of the different mixture fraction formulations on a single-shot basis in the turbulent flame, one set of collected signals is shown in Fig. 7 and the derived mixture fractions are shown in Fig. 8. Line plots of mixture fraction reveal that ξ^{N_2} and ξ^{FT} profiles generally agree around stoichiometric, although noise limitations are evident in the nitrogen Raman signal. In the turbulent flame, the N_2 Raman signal has a SNR of 6 before smoothing; this increases to 30 after contour smoothing. Instantaneous images of the turbulent flame are shown in Fig. 9, with an image size of $4.3D \times 1D$. Radial data for Figs. 7-8 are taken along the center of

each image. Additionally, scalar dissipation (two-dimensions) is computed based upon each mixture fraction formulation, where the scalar dissipation χ, is defined as $\chi \equiv 2\mathcal{D}\nabla\xi\cdot\nabla\xi$. Temperature variations are accounted for in the diffusivity $\mathcal{D}$, by the relationship $\mathcal{D}=\mathcal{D}_0\,(T/T_0)^{1.67}$. The χ^{N_2} image should be regarded as semi-quantitative due to the modest SNR of the nitrogen Raman signal. Qualitatively, the images appear similar, revealing the same main structural features, with peak scalar dissipation apparent along the edge of the main jet. The position of the stoichiometric mixture fraction contour is highlighted (black lines) in these images.

Conclusions

Two simultaneous methods of imaging mixture fraction have been investigated using planar Rayleigh, fuel Raman, and nitrogen Raman scattering in nonpremixed flames using argon/oxygen diluted methane as a fuel. The different approaches are in good agreement when applied to a laminar flame. Here, the nitrogen-temperature mixture fraction served as a guide for correcting the fuel-temperature mixture fraction for values around and lean stoichiometric. It has been shown that parameterizing specific heat, molecular weight, and Rayleigh cross section as a function of ξ^{FT} predicted from counterflow flame calculations, rather than the actual mixture fraction, dramatically improves the performance of this two-scalar approach. Under turbulent conditions (Re=15,000), the two approaches reveal differences close to the centerline, most likely a result of noise limitations of the nitrogen Raman signal. One of the shortcomings of the two-scalar approach using fuel concentration and Rayleigh scattering is the lack of a strongly varying scalar quantity around the stoichiometric contour. This work has shown that Stokes-shifted nitrogen Raman scattering is a viable candidate for a third scalar quantity to supplement the usual two-scalar approach based on measurements of fuel mass fraction and temperature. By eliminating nitrogen from the fuel stream diluent, the nitrogen mass fraction provides sufficient variation to serve as a passive scalar.

Although modest signal-noise of the nitrogen Raman make more detailed quantitative and statistical comparisons premature at this point, the current evidence indicates that this technique merits continued investigation. An added benefit of this experimental setup is that only a single laser is required. The ultimate goal of these efforts is to combine three measurements into a comprehensive mixture fraction calculation which offers significant improvement over two-scalar techniques, while maintaining the ability to compute gradient information required to accurately determine scalar dissipation.

Acknowledgments

The authors gratefully acknowledge the support of this research by the Air Force Office of Scientific Research (Grant. No. F49620-97-1-0096), and would like to thank Dr. Michael Tanoff for assistance with the counterflow flame calculations, and Dr. Robert Barlow for his useful suggestions regarding the experiments.

References

1. Long, M.B., Chu, B.T., and Chang, R.K., *Opt.Lett.* 16:958-960 (1983).

2. Escoda, M.C., and Long, M.B., *AIAA J.*, 21:81 (1983).

3. Kelman, J.B., and Masri, A.R., *Combust. Sci. and Tech.* 122:1-32 (1997).

4. Long, M.B., Fourguette, D.C., Escoda, M.C., and Layne, C.B., *Opt.Lett.* 8:244-6 (1983).

5. Masri, A.R., Dibble, R.W., and Barlow, R.S., *Prog. Energy Combust. Sci.* 22:307-362 (1996).

6. Nandula, S.P., Brown, T.M., Pitz, R.W., and DeBarber, P.A., *Opt.Lett.* 19:414-416 (1994).

7. Chen, Y.C., and Mansour, M.S. *Twenty-Sixth Symposium (International) on Combustion*, The Combustion Institute, Pittsburgh, PA, 1996, pp. 97-103.

8. Stårner, S.H., Bilger, R.W., Dibble, R.W., and Barlow, R.S., *Combust. Sci. and Tech.* 86:223-236 (1992).

9. Stårner, S.H., Bilger, R.W., Lyons, K.M., Frank, J.H., and Long, M.B., *Combust. Flame.* 99:347-354 (1994).

10. Frank, J.H., Lyons, K.M., Marran, D.F., Long, M.B., Stårner, S.H., and Bilger, R.W., *Twenty-Fifth Symposium (International) on Combustion*, The Combustion Institute, Pittsburgh, PA, 1994, pp. 1159-1166.

11. Long, M.B., Frank, J.H., Lyons, K.M., Marran, D.F., and Stårner, S.H., *Ber. Bunsenges. Phys. Chem.*, 97:1555-1559 (1993).

12. Stårner, S.H., Bilger, R.W., Long, M.B., Frank, J.H., and Marran, D.F., *Combust. Sci. Tech.* 129:141-163 (1997).

13. Kelman, J.B., Masri, A.R., Stårner, S.H., and Bilger, R.W., *Twenty-Fifth Symposium (International) on Combustion*, The Combustion Institute, Pittsburgh, PA, 1994, pp. 1141-1147.

14. Kelman, J.B., and Masri, A.R., *Combust. Sci. and Tech.* 129:17-55 (1997).

15. Marran, D.F., Frank, J.H., Long, M.B., Stårner, S.H., and Bilger, R.W., *Opt. Lett.* 20: 791-3 (1995).

16. Long, M.B., in *Instrumentation for Flows with Combustion* (A.M.K.P. Taylor, Ed.) Academic Press, 1993, p.467.

17. Namazian, M., Schefer, R.W., and Kelly, J., *Comb. and Flame*, 74:147-160 (1988).

18. Stårner, S.H., and Bilger, R.W., *Comb. and Flame*, 61:29-38 (1985).

19. Dibble, R.W., Masri, A.R., and Bilger, R.W., *Comb. and Flame*, 67:189-206 (1987).

20. Hassel, E.P., *RAMSES Spectral Synthesis Code*, University of Darmstadt, 1996.

21. Stårner, S.H., Bilger, R.W., and Long, M.B., *Combust. Sci. and Tech.* 107:195-203 (1995).

22. Bilger, R.W., Stårner, S.H., and Kee, R.J., *Comb. and Flame*, 80:135-149 (1990).

Figure Captions

1. Schematic of the three-scalar turbulent flame imaging experiment.

2. Line plot (one pixel height) showing radial variation of Rayleigh, fuel Raman, and nitrogen Raman signals in the laminar flame (Re=1600) 15 jet diameters (D=6.1 mm) downstream of the jet exit. The data represent a 50-shot average.

3. Radial variation of mixture fraction calculated from fuel-temperature (solid line) and nitrogen-temperature (short dashes) two-scalar approaches 15D downstream in the laminar flame. Previous functional dependences of parameters in ξ^{FT} overpredict the fuel-temperature mixture fraction in regions around and lean of stoichiometric (long dashes).

4. Mixture fraction calculated from strained laminar flame calculations ($100s^{-1}$) using the fuel-temperature (solid line) and nitrogen-temperature (short dashes) two-scalar approaches plotted against mixture fraction calculated using the formula proposed by Bilger [22]. The effect of fuel correction on ξ^{FT} is also shown (long dashes).

5. Measured radial Raman and Rayleigh intensities for a 100-shot average of the turbulent flame (Re=15,000) along a line 25D downstream.

6. Radial variation of mixture fraction calculated from fuel-temperature (solid line) and nitrogen-temperature (short dashes) two-scalar approaches 25D downstream in the turbulent flame (100-shot average).

7. Measured radial Raman and Rayleigh intensities for a single shot of the turbulent flame along a line 25D downstream.

8. Radial variation of mixture fraction calculated from fuel-temperature (solid line) and nitrogen-temperature (short dashes) two-scalar approaches 25D downstream in the turbulent flame (single shot).

9. Instantaneous (a) Rayleigh, (b) CH_4 Raman, (c) N_2 Raman images of the turbulent flame. Also shown are the computed mixture fraction images (d) ξ^{FT}, (e) ξ^{N_2}, (f) temperature, and scalar dissipation images (g) χ^{FT}, and (h) χ^{N_2}. Image size is 4.3D × 1D; data for line plots of Figs. 7-8 are taken along the center of each image.

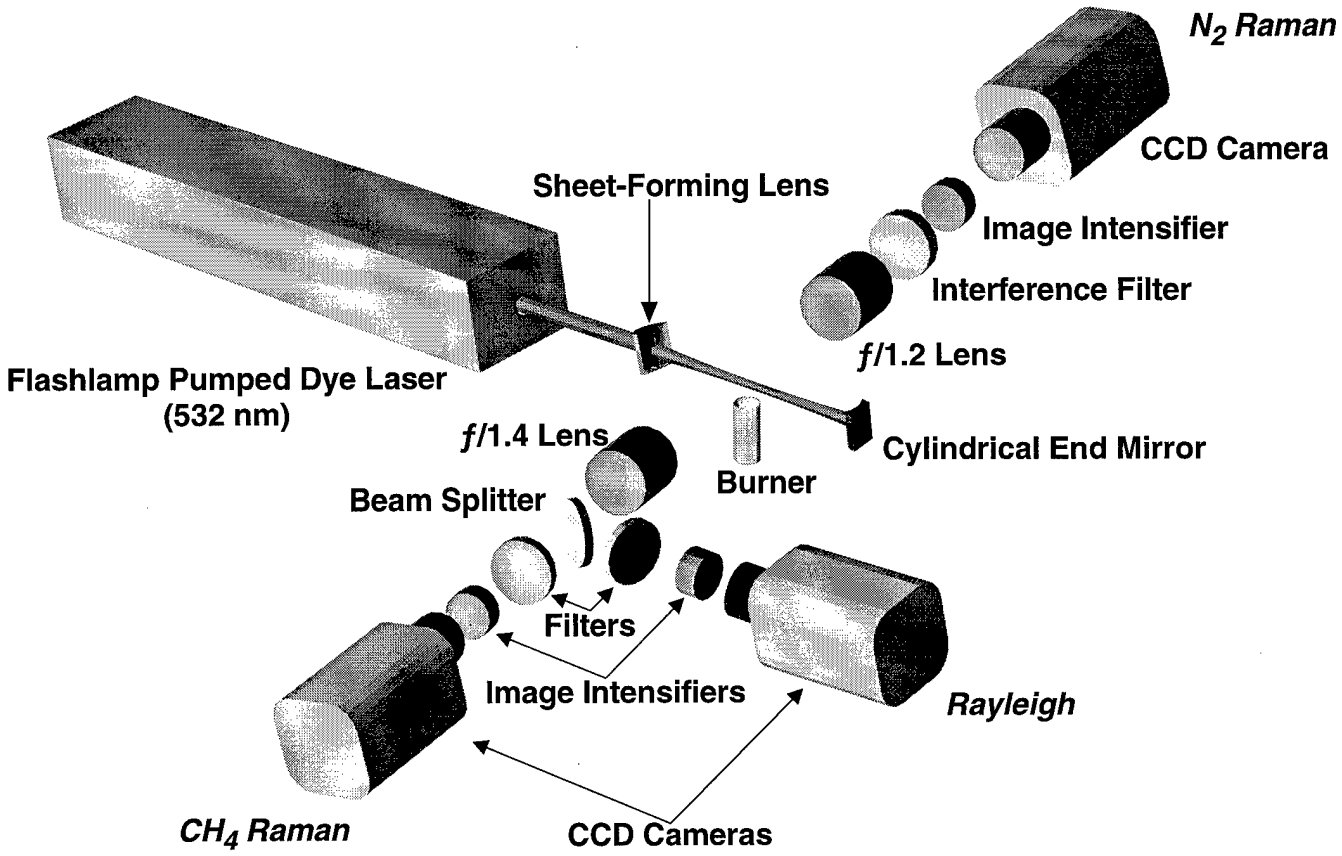
N_2 Raman
CCD Camera
Sheet-Forming Lens
Image Intensifier
Interference Filter
f/1.2 Lens
Flashlamp Pumped Dye Laser
(532 nm)
f/1.4 Lens
Cylindrical End Mirror
Burner
Beam Splitter
Filters
Image Intensifiers
Rayleigh
CH_4 Raman
CCD Cameras

Figure 1

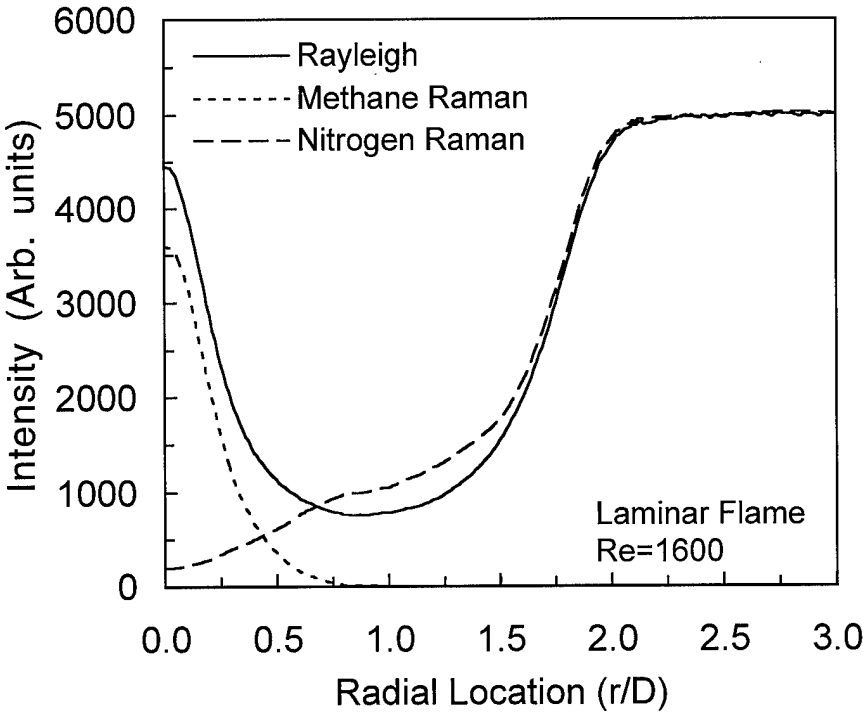
6000
5000
4000
3000
2000
1000
0
Intensity (Arb. units)
Rayleigh
Methane Raman
Nitrogen Raman
Laminar Flame
Re=1600
0.0
0.5
1.0
1.5
2.0
2.5
3.0
Radial Location (r/D)

Figure 2

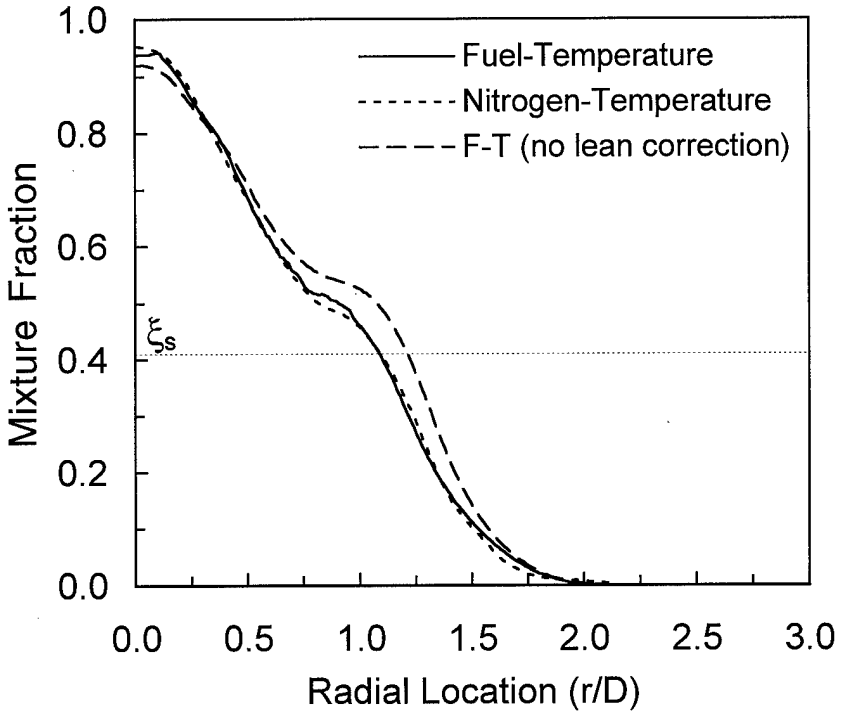
1.0
0.8
0.6
0.4
0.2
0.0
Mixture Fraction
ξ_s
Fuel-Temperature
Nitrogen-Temperature
F-T (no lean correction)
0.0
0.5
1.0
1.5
2.0
2.5
3.0
Radial Location (r/D)

Figure 3

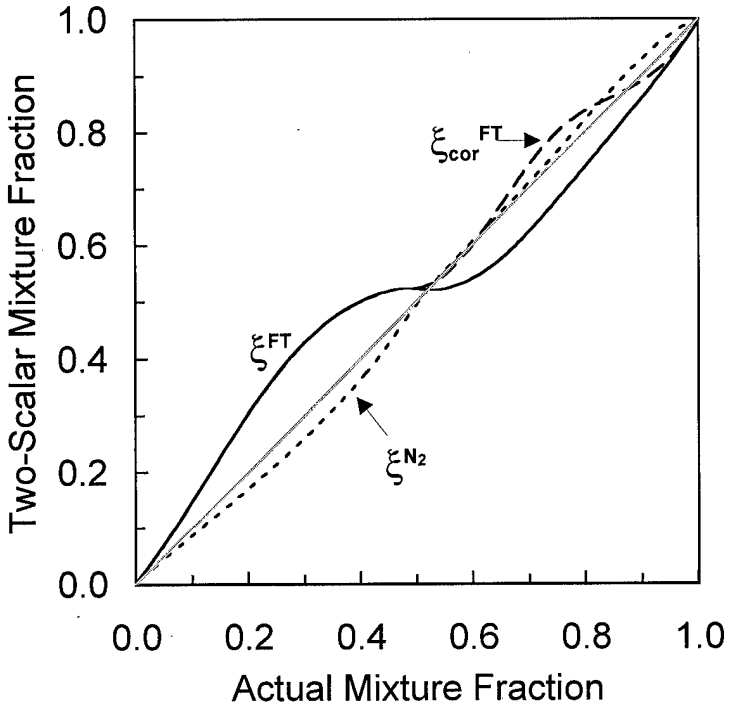
1.0
0.8
0.6
0.4
0.2
0.0
Two-Scalar Mixture Fraction
0.0
0.2
0.4
0.6
0.8
1.0
Actual Mixture Fraction
ξcor FT
ξFT
ξN2

Figure 4

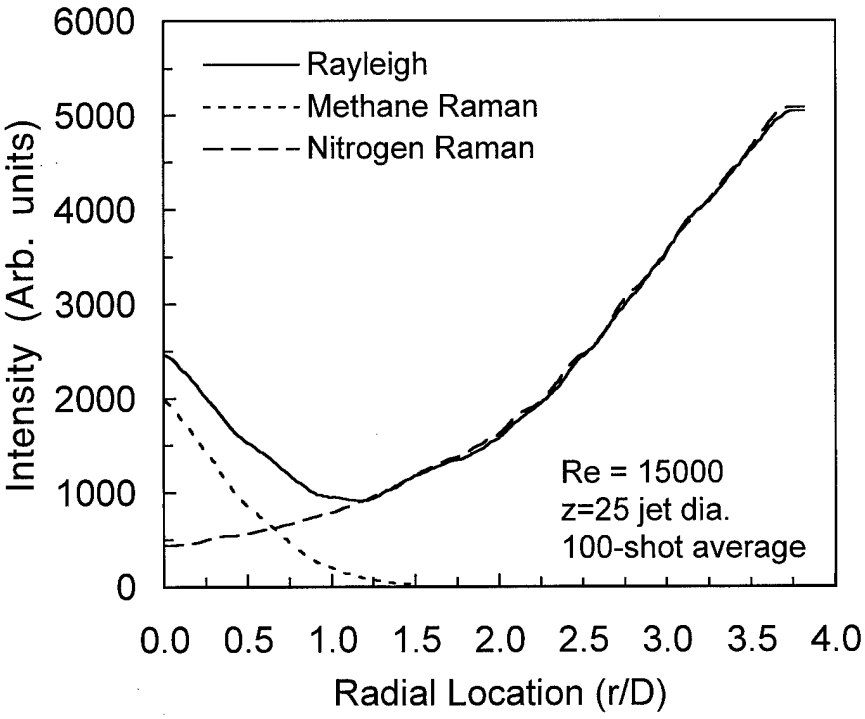
6000
5000
4000
3000
2000
1000
0
Intensity (Arb. units)
Rayleigh
Methane Raman
Nitrogen Raman
Re = 15000
z=25 jet dia.
100-shot average
0.0
0.5
1.0
1.5
2.0
2.5
3.0
3.5
4.0
Radial Location (r/D)

Figure 5

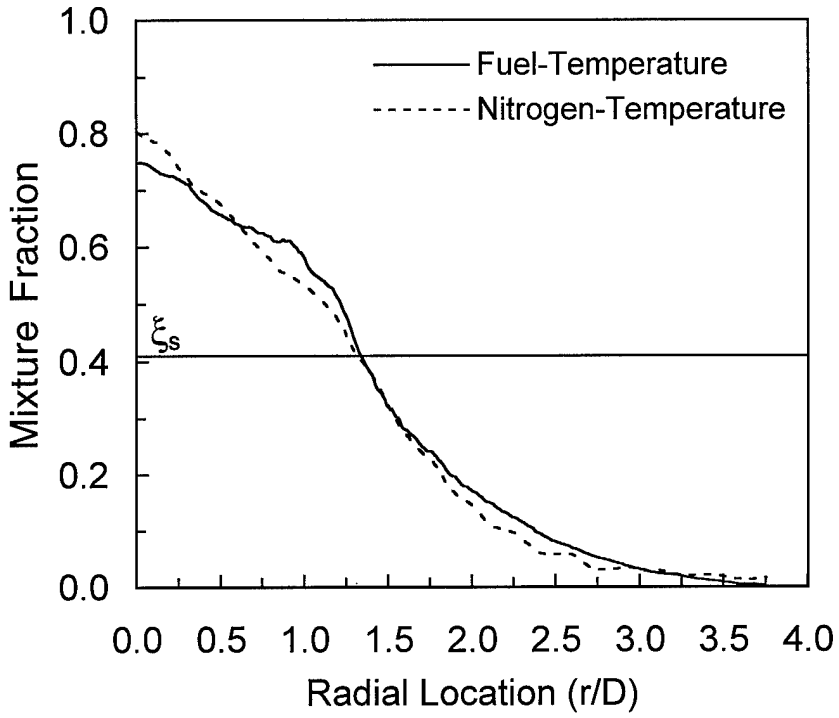
1.0
0.8
0.6
0.4
0.2
0.0
Mixture Fraction
Fuel-Temperature
Nitrogen-Temperature
ξ_s
0.0 0.5 1.0 1.5 2.0 2.5 3.0 3.5 4.0
Radial Location (r/D)

Figure 6

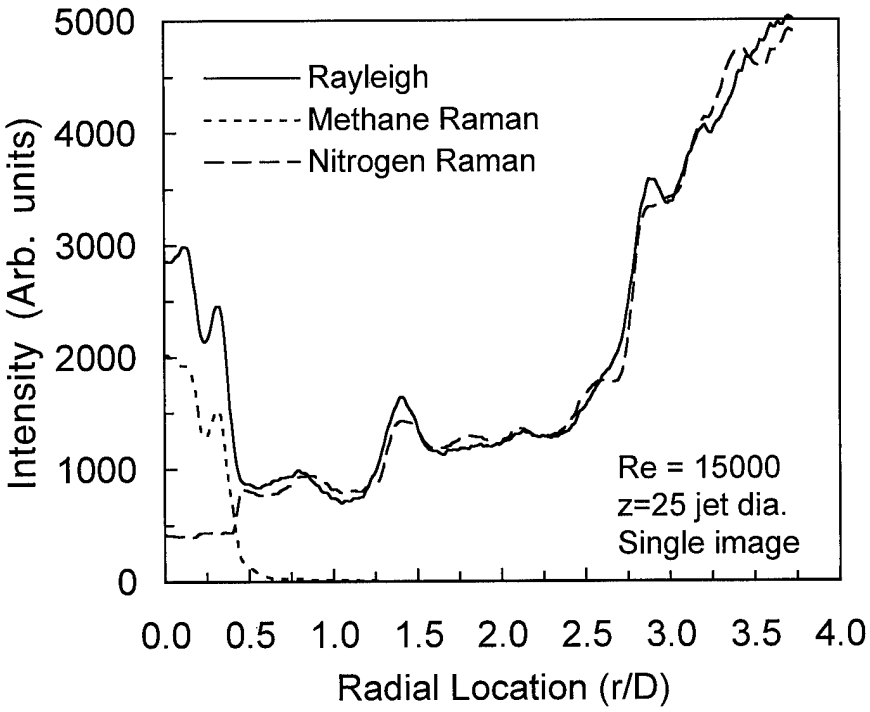
5000
4000
3000
2000
1000
0
Intensity (Arb. units)
Rayleigh
Methane Raman
Nitrogen Raman
Re = 15000
z=25 jet dia.
Single image
0.0
0.5
1.0
1.5
2.0
2.5
3.0
3.5
4.0
Radial Location (r/D)

Figure 7

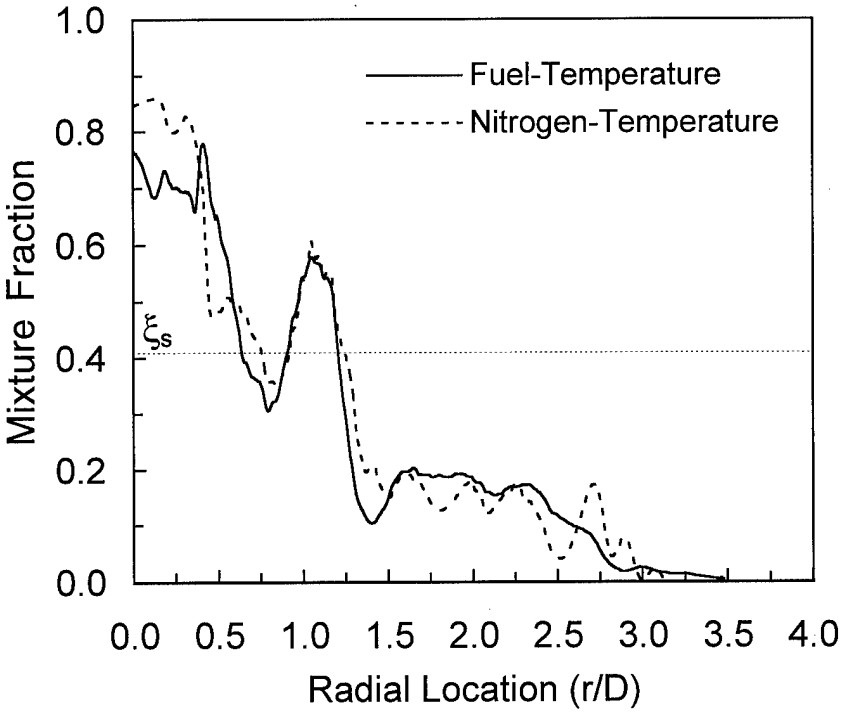
1.0
0.8
0.6
0.4
0.2
0.0
Mixture Fraction
ξs
Fuel-Temperature
Nitrogen-Temperature
0.0 0.5 1.0 1.5 2.0 2.5 3.0 3.5 4.0
Radial Location (r/D)

Figure 8

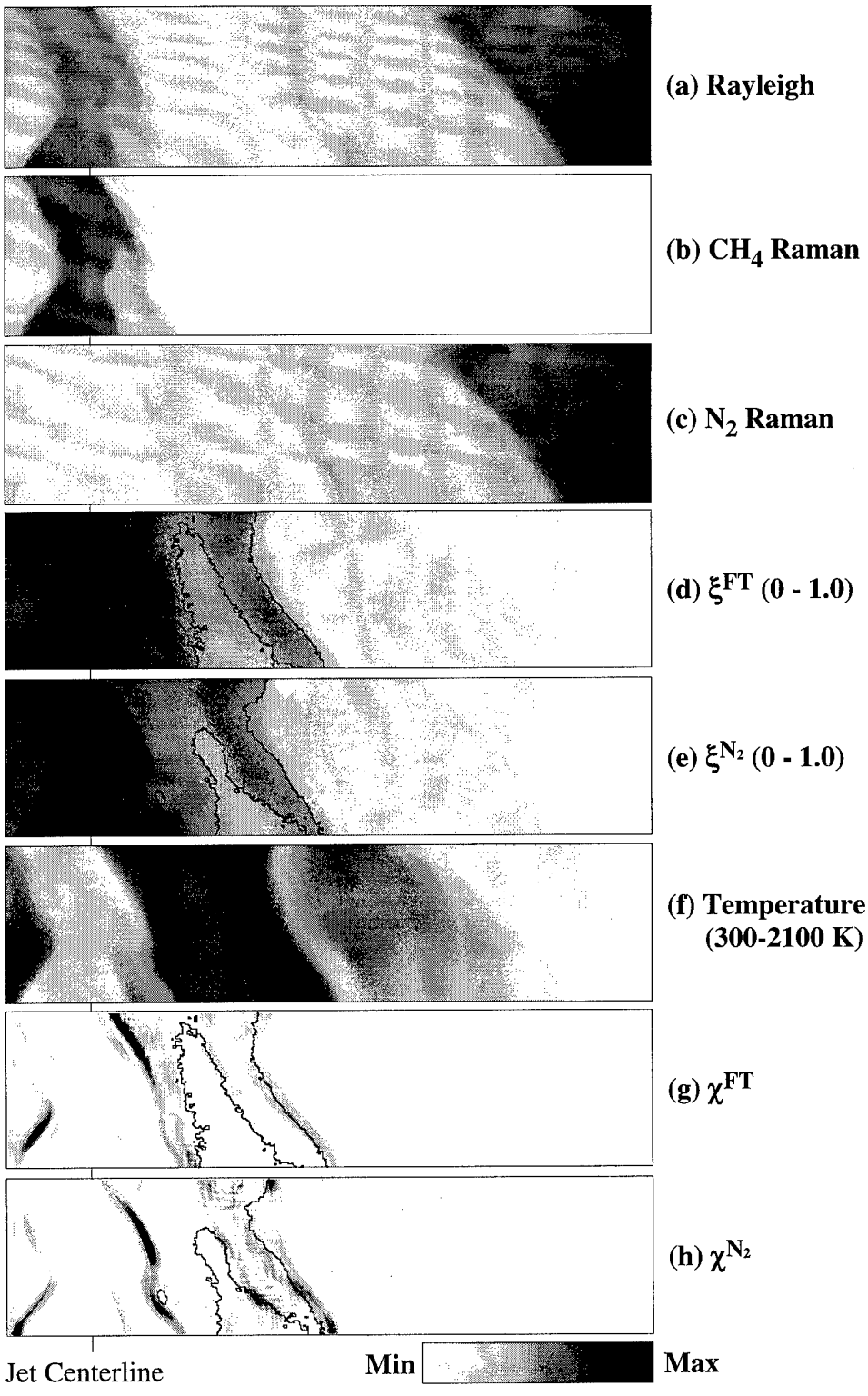
(a) Rayleigh
(b) CH_4 Raman
(c) N_2 Raman
(d) ξ^{FT} (0 - 1.0)
(e) ξ^{N_2} (0 - 1.0)
(f) Temperature (300-2100 K)
(g) χ^{FT}
(h) χ^{N_2}
Jet Centerline
Min
Max

Figure 9

Combust. Sci. and Tech., 1997, Vol. 129, pp. 141–163
Reprints available directly from the publisher
Photocopying permitted by license only

Scalar Dissipation Measurements in Turbulent Jet Diffusion Flames of Air Diluted Methane and Hydrogen

S. H. STÅRNER[a], R. W. BILGER[a,*], M. B. LONG[b], J. H. FRANK[b] and D. F. MARRAN[b]

[a]*The University of Sydney, N.S.W. 2006, Australia;*
[b]*Yale University, Conn. USA*

(Received 10 October 1996; In final form 28 July 1997)

Simultaneous two-dimensional Rayleigh and fuel Raman images have been collected in air-diluted methane and hydrogen jet diffusion flames. Temperature, fuel mass fraction and mixture fraction images are derived by a two-scalar approach based on one-step chemistry and equal species diffusivities. This enables calculation of two components of the scalar dissipation rate χ. The inherently weak Raman signal has been maximised by intra-cavity measurements, using a flashlamp-pumped dye laser. In addition, the Raman signal-to-noise ratio is drastically improved by a novel contour-aligned smoothing technique which exploits the high correlation between the Rayleigh and Raman signals.

Quantitative measurements of scalar dissipation are presented, including probability density functions for components of χ. Profiles of mean and rms mixture fraction show the usual features already documented in other published results for this type of flame. Probability density functions of ξ are close to Gaussian on the axis, and tend to bimodal at the edge of the flame. Results for the CH_4 flames indicate that the mean of χ shows little change with Reynolds number. In the H_2 flame, mean values for the axial and radial components of the scalar dissipation rate, χ, are nearly the same, indicating a more isotropic structure than in the CH_4 flames. For both fuels, the pdf of $\ln(\chi)$ on the axis is more peaky than a lognormal distribution and somewhat skewed. The profiles of $\langle\chi|\eta\rangle$ show a nonlinear dependence on mixture fraction and have no clear resemblance to the skewed, monomodal shapes seen in cold flows. In the H_2 flame there is a strong correlation between instantaneous, local values of scalar dissipation and the departure from equilibrium, as measured by temperature depression.

Keywords: Laser diagnostics; turbulent nonpremixed flames; scalar dissipation

*Corresponding author. E-mail: bilger@tiny.me.su.oz.au

1. INTRODUCTION

In an overview of recent development of techniques (Frank *et al.*, 1995; Kelmen *et al.*, 1995; Stårner *et al.*, 1994b) for measuring mixture fraction and its dissipation in turbulent flames, (Bilger, 1993a) argues that such experiments are needed not only to test the validity of flamelet models, but also to aid in the development of the Conditional Moment Closure approach (Klimenko, 1990; Bilger, 1993b), where information on the mean scalar dissipation $\langle\chi|\xi\rangle$, conditional on the mixture fraction, ξ, is vital. Bilger (1993a) also stresses that only by the use of a conserved scalar such as ξ can turbulent flame structure and statistics be directly related to non-reacting turbulent flows.

The two-scalar theory (which uses the simplifying assumptions of one-step chemistry and equal species diffusivities) on which the present work is based (Bilger, 1993c) has been validated by single-point Raman/Rayleigh measurements (Stårner *et al.*, 1992). There are several possible combinations of scalar pairs: in early experiments, a fluorescing fuel (acetaldehyde) was used, which in combination with Rayleigh scattering gave a pair of strong signals with a high signal-to-noise ratio (SNR) (Stårner *et al.*, 1994b, Frank *et al.*, 1995). This enabled good scalar dissipation data to be derived, but loss of parent fuel to intermediates was found to cause too large a departure from the one-step chemistry assumption implicit in the two-scalar method. Not only does fuel pyrolysis contribute to this loss, but also the inherently high CO production in oxygen-containing fuels such as acetaldehyde, acetone and alcohols make these fuels less compatible with the two-scalar method.

An alternative is to record directly the spontaneous Raman signal from an alkane fuel such as CH_4. This has been implemented successfully by a modified line imaging technique (Stårner *et al.*, 1994a). However, for 2D imaging the weak Raman signal has until recently proved too noisy for the purpose of obtaining χ quantitatively (Kelman *et al.*, 1995). To overcome this problem, an intracavity layout is now in use to increase the laser sheet energy, but even so, the SNR in the raw Raman image is rarely above eight. This is far from adequate for producing even qualitative scalar dissipation profiles; the Raman SNR needs to be above 30 for this purpose. Some improvement can be obtained with conventional smoothing (indiscriminately averaging over a fixed size sub-domain, "top-hat" or Gaussian) but the smoothing required to produce realistic-looking scalar dissipation profiles is so extensive that a large part of the gradient information is lost; the dissipation would be at best qualitative. However, we have exploited the

high correlation between the scalars used here (Rayleigh and fuel Raman) to align the smoothing sub-domain in the Raman image along the contours of the Rayleigh image. It is shown (Stårner *et al.*, 1995) that up to a factor of ten improvement in Raman SNR is obtainable by this method. With the present combination of intracavity layout and contour-aligned smoothing, we are able here to obtain adequate SNR even with the very weak Raman signal of the H_2 flame. The H_2 flame has the advantages that there is no soot problem and virtually no fuel loss to intermediates; the two-scalar formulation should therefore be a much better approximation to the real chemistry than in any hydrocarbon flame.

2. EXPERIMENTAL

A brief experimental outline is given here, with full details elsewhere (Marren *et al.*, 1995). The methane fuel jet is diluted with air (77 percent by volume, this results in a stoichiometric mixture fraction of 0.29) and issues vertically from a nozzle of diameter 6.1 mm into a filtered, vertical, coflowing 7.0 m/s air stream, at Reynolds numbers from 10,100 to 31,000. The C_2H_2/H_2/air stoichiometric, premixed pilot flame flow rate is adjusted so as to produce a steadily burning main flame without significant local extinction. The same fuel nozzle is used for the hydrogen flame, but without pilot; the Reynolds number is 13,500. To avoid overheating of the optics, the H_2 flame is turned down between successive laser shots, with a 'duty cycle' of some 10%.

Pulses from a flash-lamp pumped dye laser (3 μs, 532 nm) are used to obtain both Rayleigh and Raman images. The horizontal beam is formed into a 10 mm high sheet with a waist $t = 0.56$ mm, and aligned to include the flame axis. The laser output coupler is replaced by a cylindrical mirror outside the laser housing so that the flame can be placed inside the lasing cavity, yielding an increase of approximately five times in sheet energy, to between 4 and 8 J per pulse in this experiment.

The Raman signal is collected broadband with an intensified 2000^2 pixel CCD camera, gated at < 3 μs. In the Rayleigh images (collected with an intensified 576 × 384 pixel CCD camera) the object field is so placed that coflow air is included to one side, enabling corrections for shot-to-shot variation in beam intensity and spatial variation across the laser sheet. Images are matched, corrected for background and throughput, and calibrated by the use of exposures in fluid of known, uniform concentration.

The Raman data are smoothed using the contour-aligned method of Stårner *et al.* (1995).

When dealing with hydrocarbon flames, an inherent problem following from the single-step chemistry assumption in the two-scalar method is the loss of parent fuel to intermediate species. However, compensation for most of the error arising from this source can be made in the data reduction: the difference between the fuel mass fraction in the one-step scheme and that obtained from laminar flame calculations of strain rate representative of the turbulent methane flames (here 200/s) can be used to quantify the loss. In this work it is found that the simple expression $Rm = Rm_0(1 + 0.8\,\Phi^2)$ gives a close fit that is fairly insensitive to the strain rate over the range of interest. Here, $\Phi = (T - T_{\text{ambient}}) / (T_{\max} - T_{\text{ambient}})$, and Rm_0 and Rm are the raw and compensated Raman intensities, respectively. When tested in a laminar flame of the same composition (Fig. 1), it is seen that most of the 'shelf' in the raw data is filled in by the compensation. The level of compensation was not varied with the jet velocity as estimates indicate that the effect would not be significant for most of the results of interest.

It is common to quote the sheet waist thickness t as the limit to the scale of measurable scalar gradients. However, this poor resolution applies only when the local scalar gradient is orthogonal to the plane of the laser beam sheet. At the other extreme, i.e., when the scalar gradient is in the plane of

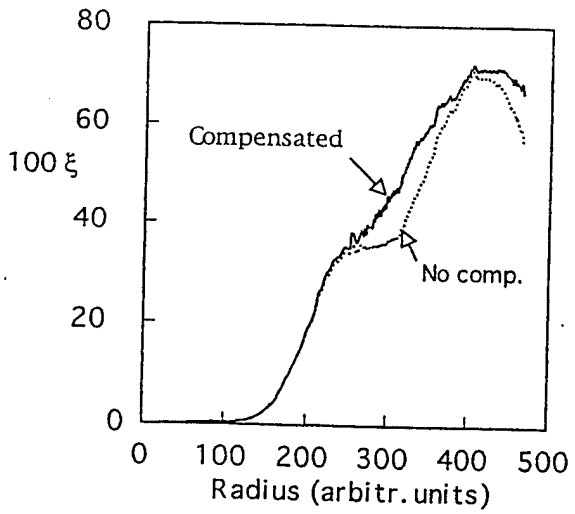

FIGURE 1 Compensation for fuel loss to intermediates in a laminar methane flame of same composition as for the turbulent flames.

the laser sheet, the resolution is limited by the pixel spacing s (here 0.0625 mm in the processed images); this would be the case in a laminar jet flame when the sheet includes the flame axis. With increasing Reynolds number, the angle between the scalar gradient and the laser beam sheet departs from zero, and a worst case would exist at very high Reynolds number when this angle is uniformly distributed in all directions. For such a case, by integrating over all orientations a simple expression is readily derived in terms of the beam thickness t and the pixel spacing s for the ensemble average of the 'resolution' ϕ ($\phi \equiv$ s for the tangential direction, $\phi \equiv t$ for the orthogonal direction): $\langle\phi\rangle = t/2 + \pi s/4$. Muss *et al.* (1994) show that for low to moderate Reynolds number, the conditions are much more favourable. It should also be recognised that no matter how high the Reynolds number, in the round jet flame the mean scalar gradient remains in the plane of the laser beam sheet, i.e., the favourable bias will persist. On this basis, we estimate that $\langle\phi\rangle \leq 0.3$ mm in the present work.

Following the arguments in Stårner *et al.* (1994a), for the H_2 flame at Re = 13,500 the Kolmogorov scale κ is estimated as 0.074 mm on the axis, so $\langle\phi\rangle/\kappa = 4.1$. In isotropic, isothermal turbulence it has been suggested (Tennekes, 1973) that energy dissipation peaks at around 30κ. This is unlikely to apply to scalar dissipation in this non-isotropic, reacting jet flow: a value of 20 κ for the scalar dissipation peak is indicated in Stårner *et al.* (1994a), and resolution to 5 κ as sufficient to capture essentially all of the scalar dissipation. At the radius where the mean temperature peaks, κ = 0.142, mm yielding $\langle\phi\rangle/\kappa = 2.1$. For the air diluted methane flame these authors give an estimate of 0.095 mm for the Kolmogorov scale on the centreline at jet Reynolds number of 20,600. The resolution in these flames should thus be adequate even at the highest Reynolds number of 31,100.

To test the sensitivity of the computed scalar dissipation to the effective resolution of the optics system, it is useful to reduce the resolution artificially by increasing the pixel size: using the hydrogen flame results, the corrected Rayleigh and Raman images are average ('binned'); then the mean scalar dissipation in the radial direction, $\langle \chi_r \rangle$, is computed. Figure 2 shows that the relative reduction in $\langle \chi_r \rangle$ is fairly large for the first increase in pixel size, from 0.0625 to 0.125 mm. At this scale the contribution to $\langle\chi_r\rangle$ should be negligible, so this reduction is likely to be due to removal of pixel-to-pixel signal noise; it is seen that the attenuation of $\langle\chi_r\rangle$ is much the same on the axis and in the hot zone, as may be expected if it is random noise only that is removed. By contrast, on again doubling the pixel size to 0.25 mm, the attenuation is much smaller. The relative attenuation is now also larger on the axis, where the integral scale is smaller (Kelman *et al.*, 1995). This is a

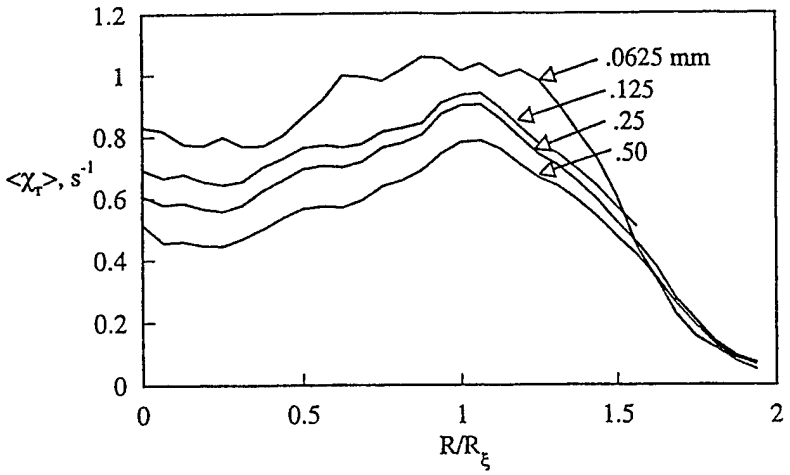

FIGURE 2 Effect of resolution (pixel size in the object plane) on computed radial component of mean scalar dissipation, $\langle \chi_r \rangle$ in the H_2 flame. The radius R is normalised by the mixture fraction half-radius, R_ξ. Average over 25 images.

good indication of the start of genuine attenuation of $\langle \chi_r \rangle$. Further pixel size doubling to 0.5 mm results in more substantial attenuation, and again the relative attenuation is largest on the axis (≈20 %). Extrapolation of the data at 0.125, 0.25 and 0.5 mm pixel size to zero indicates that attenuation at 0.125 mm is less than 2% in the hot zone, and around 10% on the axis. The results presented below are given for 0.0625 mm size, and it thus appears that residual noise more than compensates for the attenuation, (i.e., measured $\langle \chi \rangle$ is above the true level) but errors due to noise and limited resolution should be no larger than 15%.

As an alternative measure of the noise level on the computed scalar dissipation, the axial component of χ has been measured in a laminar H_2 flame, where the mean gradient of ξ is negligible. In the turbulent flame, this component is found to be typically seven times the measured value in the laminar flame. This is consistent with the deduction made above that the initial attenuation of $\langle \chi_r \rangle$ in Figure 2 (pixel size increased from 0.0625 to 0.125 mm), around 15 %, is due to high-frequency noise removal.

Typically, 100 images are used to calculate statistical quantities in this paper using data from a window 1 mm wide in radius and 8 mm in axial length to give a total of about 200,000 measurements for each spatial "point". Errors in nongradient statistics such as means and standard deviations of mixture fraction, fuel mass fraction and temperature arise from fundamental uncertainties in the technique rather than on sampling

statistics. For means these are estimated as 90% confidence intervals of ±0.02 for fuel mass fraction and mixture fraction and ±5% of the absolute temperature for temperature. For standard deviations the errors are likely to be somewhat lower.

2.1. The Two-Scalar Method

Full details of the two-scalar technique for deriving mixture fraction data can be found in Bilger, (1993c) and Stårner *et al.* (1992, 1994a). Briefly, in a two-stream, adiabatic, reacting flow, using assumptions of homogeneous inlet conditions and equal Lewis numbers, and simplifying the kinetics to a one-step reaction between fuel and oxidant, the fuel mass fraction Y_f (here defined as including any dilutant such as 70 % air in the methane flame) and enthalpy $H = c_p T/Q$ are used to form the conserved scalar $\beta = Y_f + c_p T/Q$, where c_p is the specific heat at constant pressure, and Q the lower heat of combustion of the diluted fuel. The mixture fraction ξ is then defined by

$$\xi = \frac{\beta - \beta_2}{\beta_1 - \beta_2} = \frac{Y_f + c_p(T - T_2)/Q}{Y_{f,1} + c_p(T_1 - T_2)/Q} \tag{1}$$

where subscripts 1 and 2 denote the fuel and air streams.

Rayleigh measurements are used to obtain temperature: $T \sim \sigma / Ry$, where Ry is the Rayleigh signal. The Rayleigh cross section, σ, the mole weight, W, and c_p vary with ξ and T, and hence require an iterative data reduction scheme; predictions for an opposed flow laminar flame are used to determine σ and W for the burnt state. Values of c_p are based on known concentrations of reactants and products. The Raman signal, Rm, measures the fuel concentration. With some arithmetic, Eq. (1) can be cast in a form which expresses the mixture fraction as a function of Rm and Ry:

$$\xi = \frac{C_1}{W}\frac{\sigma}{Ry} Rm + c_p/Q\left(\frac{\sigma}{Ry} - T_2\right) \tag{2}$$

where C_1 is a calibration constant.

3. RESULTS AND DISCUSSION

Computed profiles of mean and rms of mixture fraction, fuel mass fraction and temperature in the methane flames are shown in Figures 3 and 4 (Favre

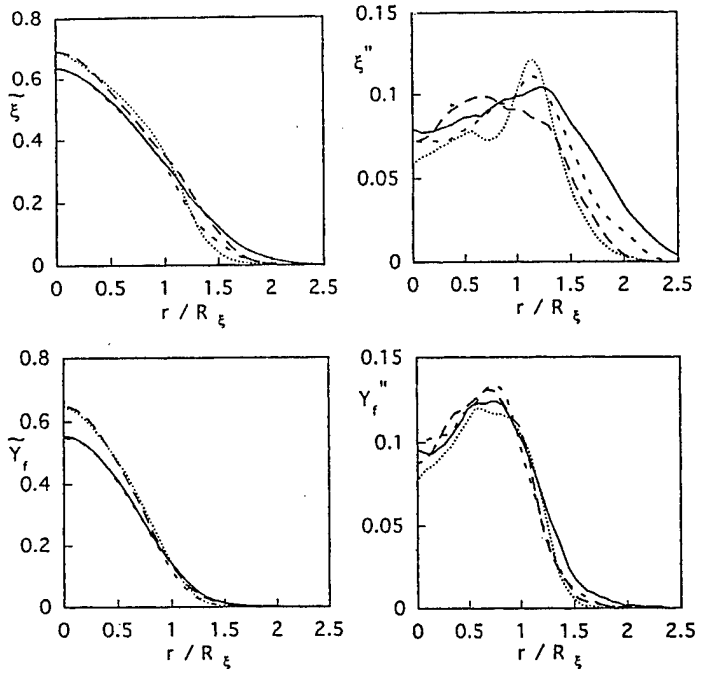

FIGURE 3 CH_4 flames: radial profiles of mean and rms fluctuation of mixture fraction ξ and fuel mass fraction Y_f, – – – Re = 10,100; · · · · · Re = 14,300; ----- Re = 21,300; —— Re = 31,100.

averaged, denoted by tilde overbars), at an axial location of 25 jet diameters (D) from the nozzle. The profiles of ($\tilde{\xi}$) and ($\tilde{Y}_f$)are similar to those for the diluted CH_4 flame in Stårner *et al.* (1994a) but centreline values are higher, and turbulence levels are lower. It is thought that the main reason is the absence of local extinction in the present case. (An extinguished flame would approximate to a cold jet which would mix down more rapidly). The mean temperature profiles in Figure 4 are quite smooth, and the peak temperature decreases as the jet Reynolds number increases. However, the rms fluctuation shows a local minimum at the radius of mean stoichiometric composition. This feature is apparent at all Reynolds numbers and is no artefact: it can also be seen in Drake *et al.* (1984) in the upstream region of a H_2 flame with jet Reynolds number 8,500. In downstream locations it is not present, and we may speculate that it is the effect of suppression of the turbulence Reynolds number in the zone of mean stoichiometric composition, just inside the radius where the onset of intermittency markedly increases the temperature fluctuations. In the flame of Stårner *et al.* (1994a) the temperature rms does not show a local minimum; there are two

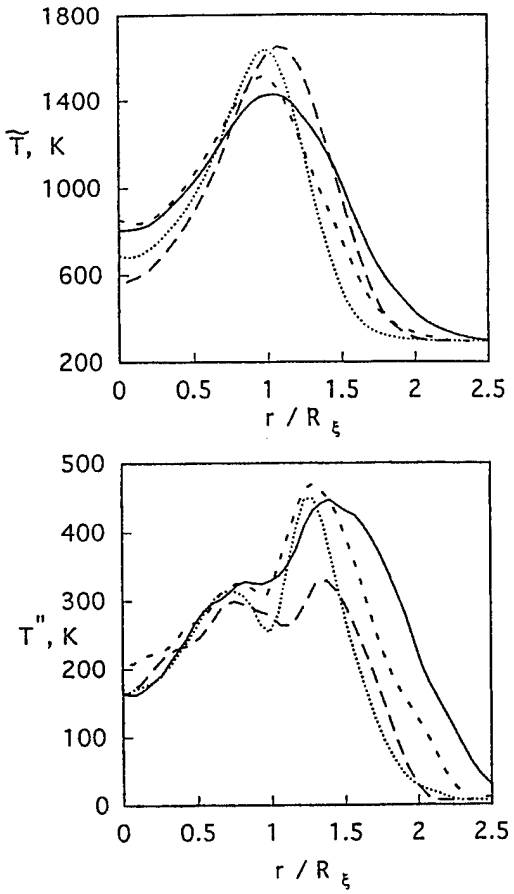

FIGURE 4 CH_4 lame: radial profiles of mean and rms fluctuation of temperature, T. – – – Re = 10,100; · · · · Re = 14,300; ---- Re = 21,300; —— Re = 31,100.

differences between that flame and the present ones which may account for this: firstly, the larger dilution in Stårner *et al.* (1994a) results in larger stoichiometric mixture fraction which shortens the flame, so that although measurements are made at the same axial position, it is equivalent to a position further downstream in the present flame. Secondly, the flame in Stårner *et al.* (1994a) is half extinguished at the neck, which can be expected to alter the turbulence distribution.

For the hydrogen flame, corresponding profiles of mean and rms of mixture fraction, fuel mass fraction and temperature are shown in Figure 5, at 20 D from the nozzle. Measurements in a laminar H_2 flame during these experiments (not shown here) yield a radial profile of ξ that is smooth and

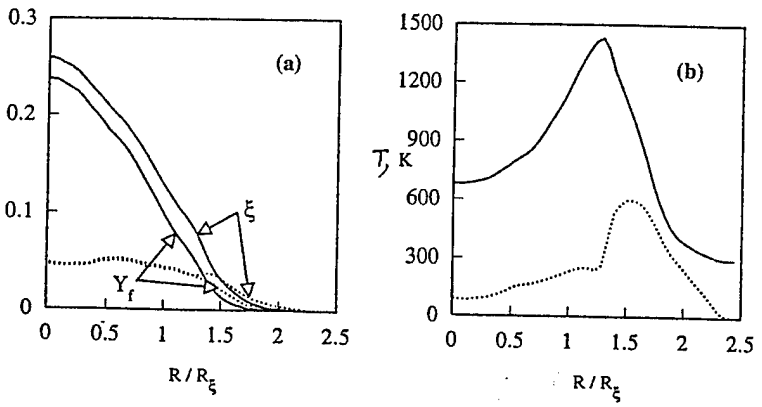

FIGURE 5 H_2 flame: radial profiles of density-weighted mean (—) and rms fluctuation (···) of (a) mixture fraction ξ and fuel mass fraction Y_f; (b) temperature, T.

has no marked irregularity such as occurs in the methane of Figure 1 around stoichiometric. This is an indication that the calculation of ξ is not seriously affected by the limitations of the two-scalar method. The mean temperature profile in Figure 5 has a marked peak, and its rms fluctuation rises steeply at the radius of mean stoichiometric composition, as also found by Drake *et al.* (1984). The rapid rise in the rms of T at $R/R_\xi = 1.3$ (where R_ξ is the mixture fraction half-radius) is mainly an effect of intermittency, but may also in part be associated with a marked departure from equilibrium which manifests itself around stoichiometric composition and results in a wider range of T.

For both fuel types there is evidence in the scatter plots of temperature in Figures 6 and 7 of marked departure from equilibrium, as also seen in Barlow and Carter (1994). For the hydrogen flame the scatter plots correspond fairly well with the prediction shown for a laminar counter-flow flame at strain rate 1000 s^{-1}. Such differences as can be seen are thought to be the combined effects of higher (and fluctuating) strain rate in the turbulent flame, calibration uncertainty and the assumptions of one-step kinetics and equal species diffusivities. The scatter plots for the instantaneous scalar dissipation that are shown here assume that the azimuthal component is equal to the radial component. While this assumption should be accurate for conditional and unconditional values, it will overestimate departures from such means. This assumption is also used in later figures and those results should also be treated with caution.

The probability density functions (pdfs) of T in Figures 8 and 11 show largely the expected distribution in the outer shear layer, with an inter-

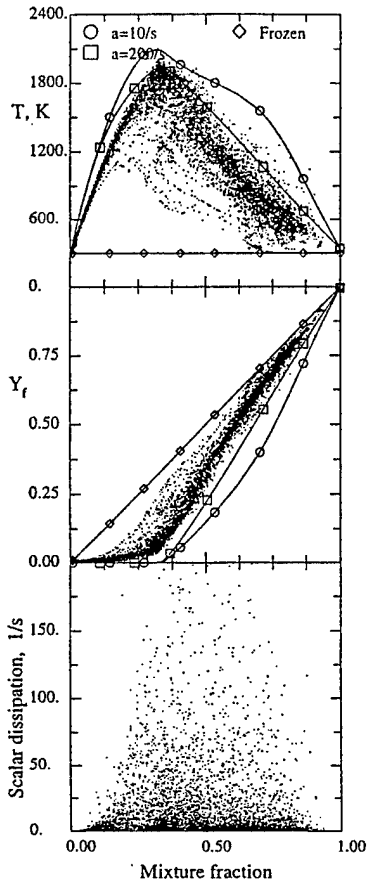

FIGURE 6 CH_4 flame: Scatter plots of temperature, T, and fuel mass fraction, Y_f, and scalar dissipation, χ conditional on mixture fraction, with points collected equally from all radii. Re = 21,300. Lines denote laminar flame calculations at strains 10 and 200 s^{-1}.

mittency peak at ambient temperature. The pdf of fuel mass fraction in Figure 9 is somewhat more bimodal in the outer layer than those of T. The corresponding pdfs of ξ (Figs. 10 and 11) are close to Gaussian on the axis, and tending towards bimodal at the edge of the flame. There is some indication in the methane flames (Fig. 10) of distortion of $p(\xi)$ around stoichiometric, in particular at low Reynolds number, most likely due to loss of parent fuel to intermediates and the imprecise attempt to compensate for this effect (Fig. 1).

Mean and rms values of the axial and radial components of scalar dissipation are shown in Figures 12 and 13. In the CH_4 flames the axial component, $\langle \chi_x \rangle$, is somewhat larger than the radial component, $\langle \chi_r \rangle$ on the

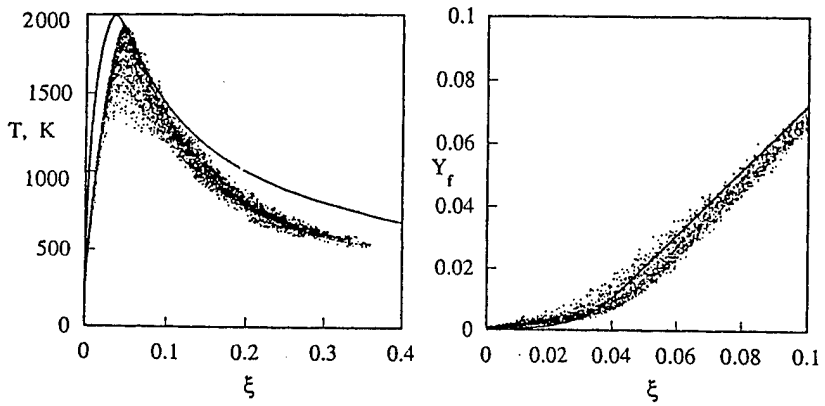

FIGURE 7 H_2 flame: scatter plots of temperature, T, and fuel mass fraction, Y_f, conditional on mixture fraction, with points collected equally from all radii. Lines denote laminar flame calculations at strain $1000\,s^{-1}$.

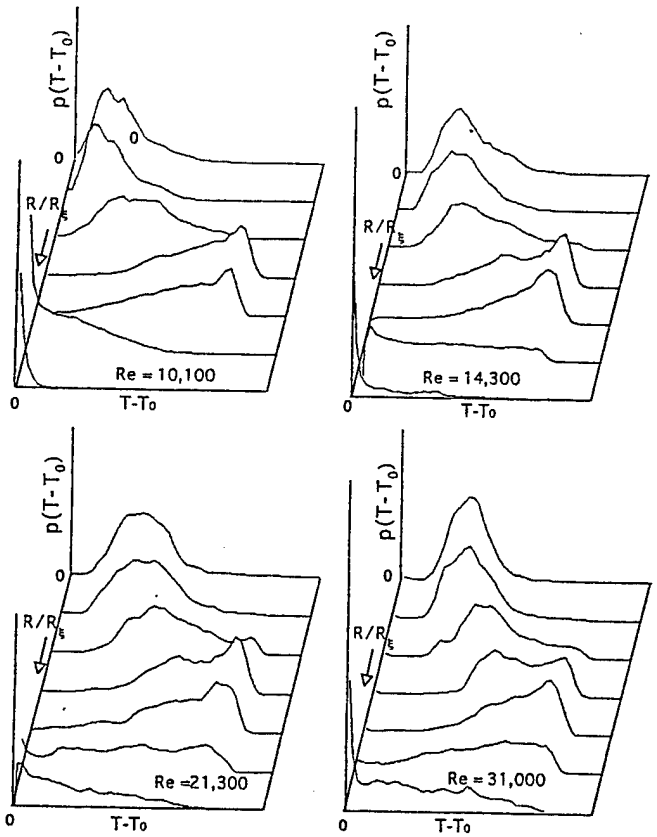

FIGURE 8 CH_4 flames: probability density of temperature T (arbitrary units) at various radii (uncalibrated).

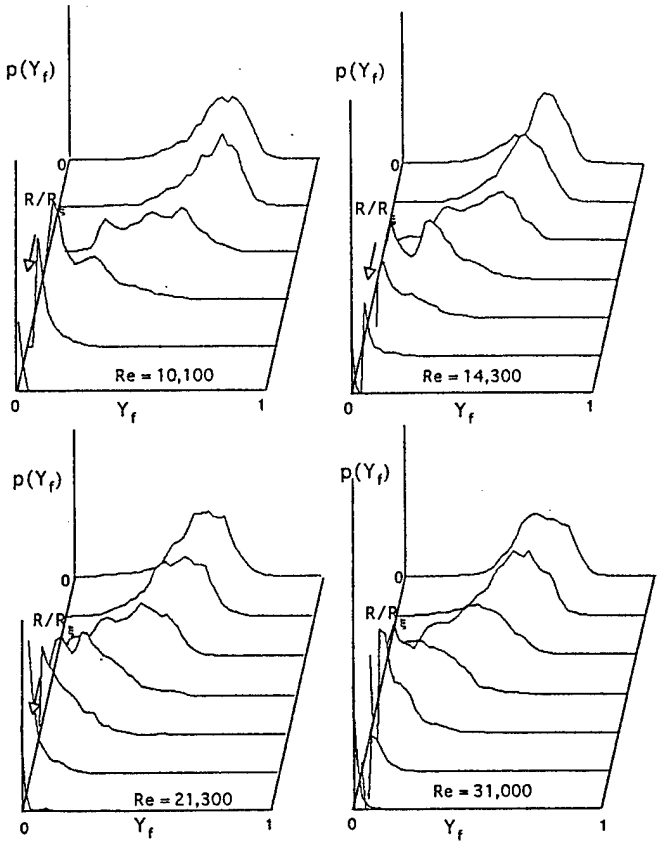

FIGURE 9 CH_4 flames: probability density of fuel mass fraction Y_{fu} (arbitrary units) at various radii (uncalibrated).

axis, whilst in the shear layer $\langle \chi_r \rangle$ grows to nearly twice $\langle \chi_x \rangle$. Results for the air-diluted CH_4 flame of Stårner *et al.* (1994a) show a similar, anisotropic structure. The rms of the components of χ in Figure 12 is around three times the corresponding mean; this is somewhat more than reported in Stårner *et al.* (1994a). It is most noteworthy that there is very little variation with the jet Reynolds number. This has also been observed by Kelman and Masri (1996) for similar flames. For self-similar flows it would be expected that the scalar dissipation would be proportional to the jet velocity divided by the jet diameter at a fixed number of jet diameters downstream. Because of the coflow, the flow here is not self similar: the spreading rate increases with jet velocity and the mixing profiles also change. This probably accounts for the lack of variation in the scalar dissipation values, but the result should

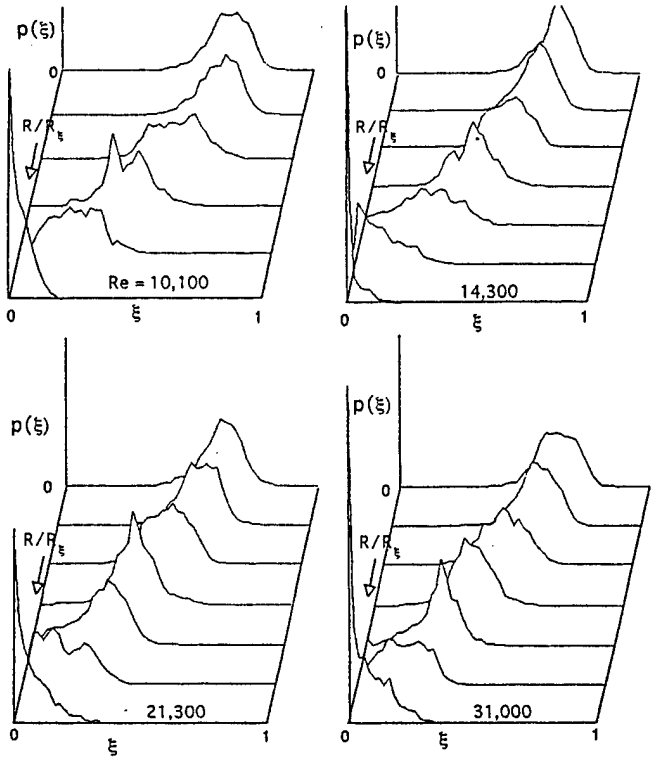

FIGURE 10 CH_4 flames: probability density of mixture fraction ξ (arbitrary units) at various radii (uncalibrated).

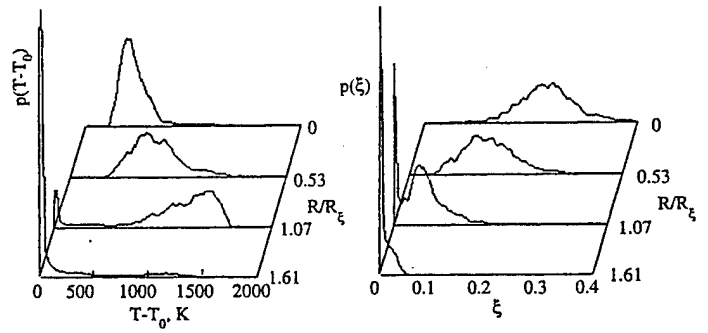

FIGURE 11 H_2 flame: probability density of temperature and mixture fraction (arbitrary units) at various radii. The radius R is normalised by the mixture fraction half-radius, R_ξ.

be treated with some caution. In the H_2 flame of Figure 13 the shear layer value of $\langle \chi_r \rangle$ grows to only 1.3 $\langle \chi_x \rangle$; this is a more isotropic structure than in the CH_4 flames. It is not obvious why this should be so, especially as the H_2

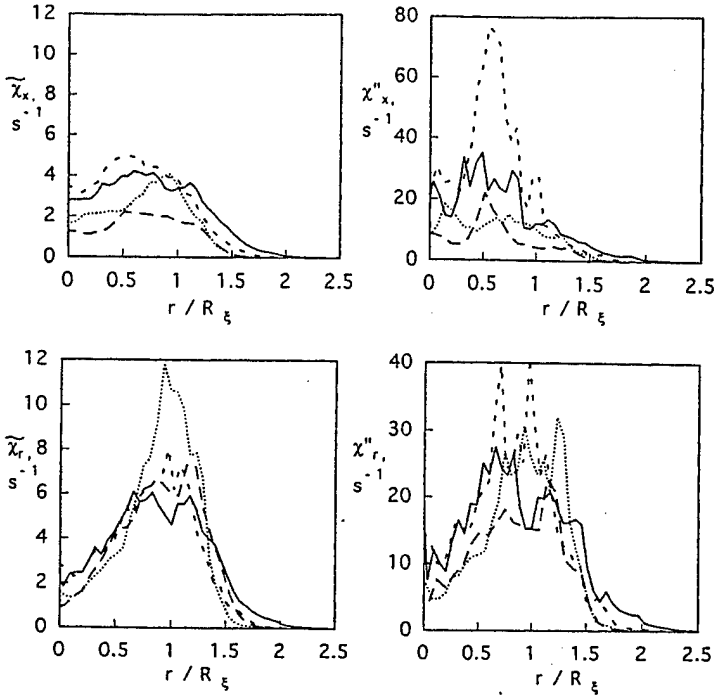

FIGURE 12 CH_4 flames: radial profiles of mean and rms fluctuation of scalar dissipation: components χ_x and χ_r. – – – Re = 10,100; · · · · Re = 14,300; ----- Re = 21,300; —— Re = 31,100.

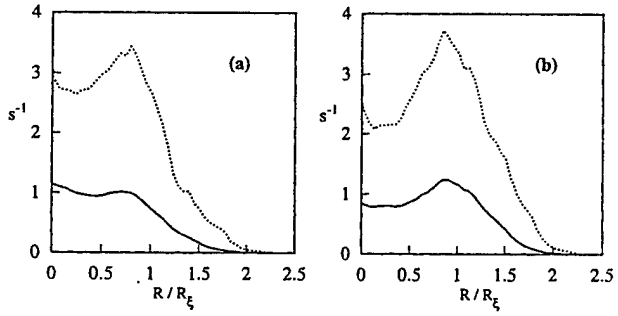

FIGURE 13 H_2 flame: radial profiles of mean (—) and rms fluctuation (· · · ·) of scalar dissipation χ: (a) axial component; (b) radial component.

flame has a rather low Reynolds number. There are, however, two marked differences between these flames: in the H_2 flame the density is lowest on the centreline, and the stoichiometric contour lies at the outer edge of the shear layer, whilst in the CH_4 flames the stoichiometric contour (and minimum

density) lie well inside the shear layer (Stårner *et al.*, 1990). The rms/mean for each component in the H_2 flame is around 3; this is close to the results for the CH_4 flames in this paper.

The pdfs of $\ln(\chi_x)$ and $\ln(\chi_r)$ on the axis (Figs. 14 and 15) are more peaky than the lognormal distribution and somewhat negatively skewed. In the shear layer, the effect of intermittency can be seen. A peaky distribution is also evident in Rayleigh scattering measurements in H_2 flames by Muss *et al.* (1994), but the sign of the skewness for their undiluted H_2 flame is positive. By contrast, results by Namazian *et al.* (1988) in the upstream region of a cold CH_4 jet (employing Raman measurements) show a close fit to the lognormal distribution. The observed negative skewness on the axis in

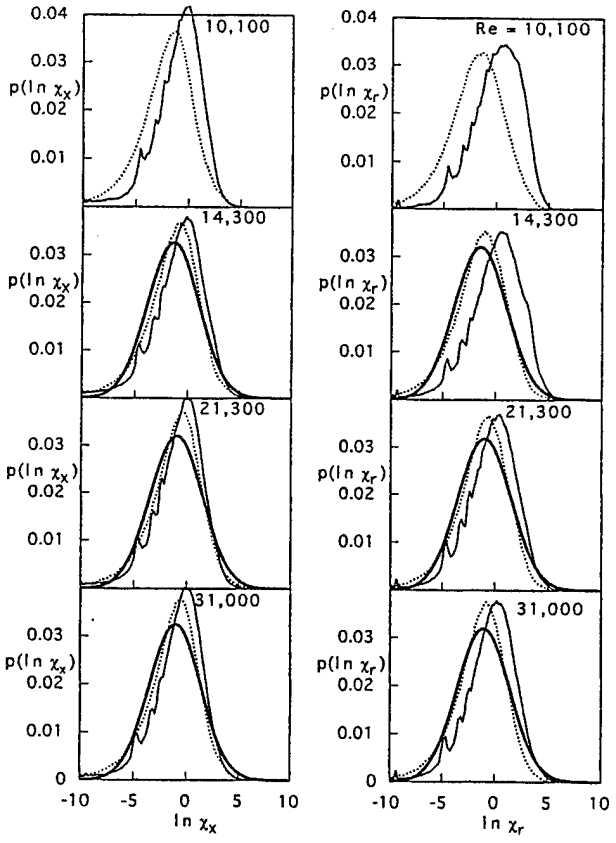

FIGURE 14 CH_4 flames: probability density of axial (left) and radial component of scalar dissipation χ: —— $R=0$; ···· $R/R_\xi=1.07$. Also shown is the lognormal distribution with mean and rms as for $R=0$.

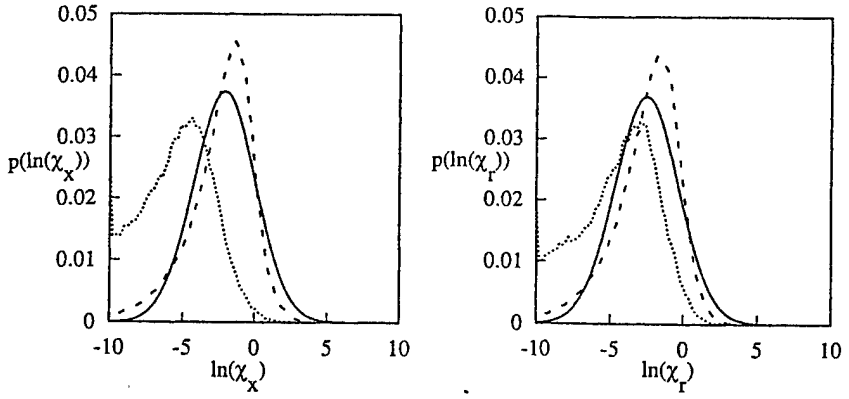

FIGURE 15 H_2 flame: probability density of axial (left) and radial component of scalar dissipation χ: —— $R=0$; ···· $R/R_\xi=1.07$. Also shown is the lognormal distribution with mean and rms as for $R=0$.

the present work may be a feature of the upstream distribution of scales and scalar dissipation in a combusting jet: on the axis the scales are smaller than in the hot zone surrounding the shear layer, and the occasional appearance on the axis of hot fluid (with large scales and low χ) would create a tail in the pdf towards low χ. It should be noted, however, that as limited spatial resolution will have the largest averaging effect on samples with high χ (high scalar gradients being associated with smaller scales), the effect is to clip the pdf at high χ; this would contribute to an artificial peakiness.

Figures 16 and 17 show conditional mean scalar dissipation, $\langle\chi|\eta\rangle^*$, conditional on mixture fraction, and normalised by its local unconditional mean. Here η is the independent sample space variable corresponding to the dependent mixture fracture variable, ξ. The profiles of $\langle\chi|\eta\rangle^*$ have no clear resemblance to those in cold flows, such as the skewed, monomodal shapes in jets by Kailasnath *et al.* (1993) or the u-shapes in the grid flow in a mean transverse temperature gradient by Jayesh and Warhaft (1992). The upturn in $\langle\chi|\eta\rangle$ at large η could be caused by the rare appearance of fluid of simultaneously large ξ and χ; a strong indication of this is reported by Jayesh and Warhaft (1992).

Departure from equilibrium (i.e., temperature depression in the scatter plot) is normally assumed to be caused by locally high values of χ. If this is the case, one should expect a clear negative correlation between T and χ (provided that the measurement resolution is adequate). This is indeed so: in the H_2 flame of Figure 18 the correlation coefficient $C_{T\chi}|\eta$ (conditional on mixture fraction) has a minimum of -0.44 slightly rich of stoichiometric.

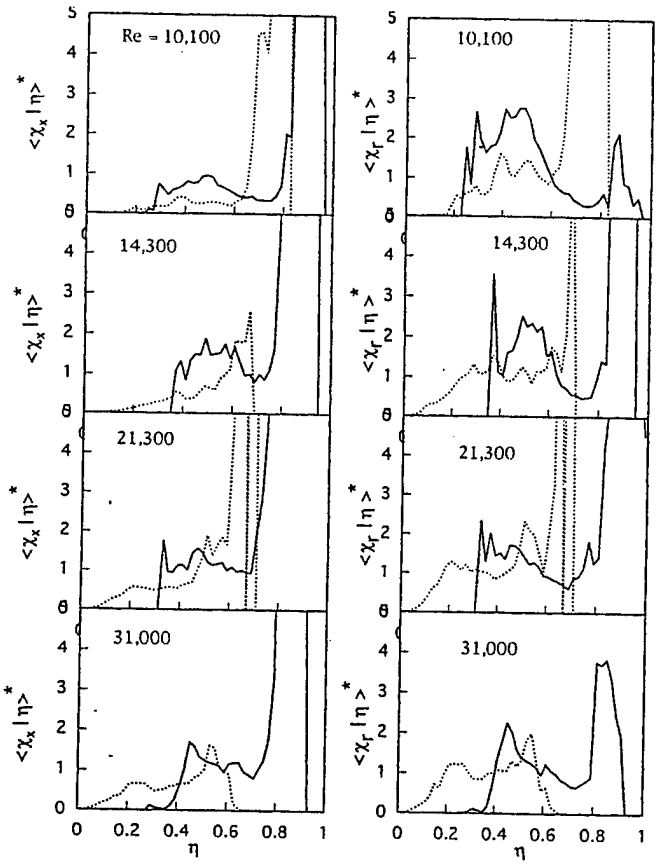

FIGURE 16 CH_4 flames: Mean scalar dissipation components, conditional on mixture fraction ξ taking the value η, and normalised by their local unconditional means. Data collected near the axis and in the shear layer. —— $R/R_\xi = 0-0.25$; $\cdots$ $R/R_\xi = 0.75-1.25$.

Here χ is calculated by assuming that the radial and azimuthal components are equal, i.e., $\chi = \chi_x + 2\chi_r$ (Stårner *et al.*, 1994a) and the caution given earlier in using this for non mean quantities applies. If we assume that the rms of χ is inflated by residual noise, as indicated in Figure 2, then the correlation would be straightened by this effect, perhaps compensating for the error introduced by assuming that the radial and azimuthal components are equal for fluctuations. Outside the main reaction zone the correlation is seen to weaken. This is to be expected where the flow is convection dominated and the very low reaction rate (whether inhibited or not) is insignificant. The weak positive correlation for $\eta > 0.2$ arises as a calculation artefact: because finite mixture fraction intervals, $\delta\eta$, must be used in

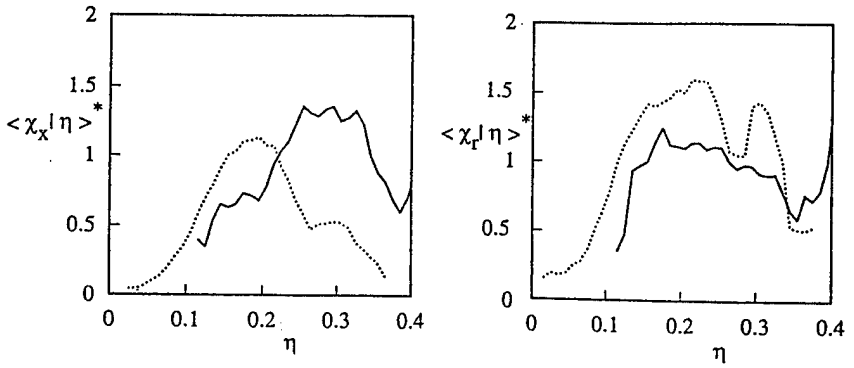

FIGURE 17 H_2 flames: Mean scalar dissipation components, conditional on mixture fraction ξ taking the value η, and normalised by their local unconditional means. Data collected near the axis and in the shear layer. —— $R/R_\xi = 0-0.25$; ···· $R/R_\xi = 0.75-1.25$.

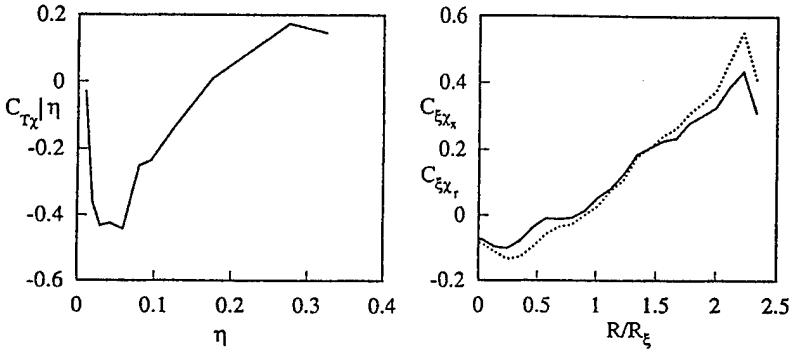

FIGURE 18 H_2 flame: (a): Correlation coefficient of temperature and scalar dissipation, $C_{T_\chi}|\eta$, conditional on mixture fraction. The radial and azimuthal components of χ are assumed equal, so that $\chi = \chi_x + 2\chi_r$. (b): Radial variation of correlation coefficients of mixture fraction ξ and scalar dissipation components χ_x(—) and χ_r(---).

computing $C_{T_\chi}|\eta$, and because at large η $dT/d\eta$ and $d\chi/d\eta$ have the same sign, a spurious 'gradient transport' correlation arises which can be minimised only at the cost of increased scatter as $\delta\eta \to 0$.

If the assumption is made that χ and ξ are independent variables, the joint pdf of χ and ξ can be modelled as the product of two separate pdfs, permitting major computational simplification. The correlation coefficient $C_{\chi\xi}$ (shown in Fig. 18 separately for the axial and radial components of χ) appears to support this assumption in the inner shear layer. For $R/R_\xi > 1.2$, however, $C_{\chi\xi}$ becomes substantial. Similar results for a CH_4 flame can be found in Stårner *et al.* (1994a), and for a cold jet in Namazian *et al.* (1988). It should be noted that a near zero correlation coefficient is not sufficient to

establish independence of χ and ξ. As seen in Figure 17 the interdependence is non-linear and the conditional average scalar dissipation differs significantly from the unconditional average for much of the range of η of interest.

One important aspect of Conditional Moment Closure modelling is that the number of spatial coordinates often can be reduced. It has been shown (Bilger, 1993b) that in reacting, constant-density flows, conditioning on the mixture fraction renders mean scalar quantities independent of the cross-stream coordinate. Recent development in CMC modelling (Klimenko *et al.*, 1995) indicate that the integral of $\langle\chi|\eta\rangle$ across the flow,

$$\int_0^\infty \langle\chi|\eta\rangle p_\eta(\eta) r dr \Big/ \int_0^\infty p_\eta(\eta) r dr \tag{3}$$

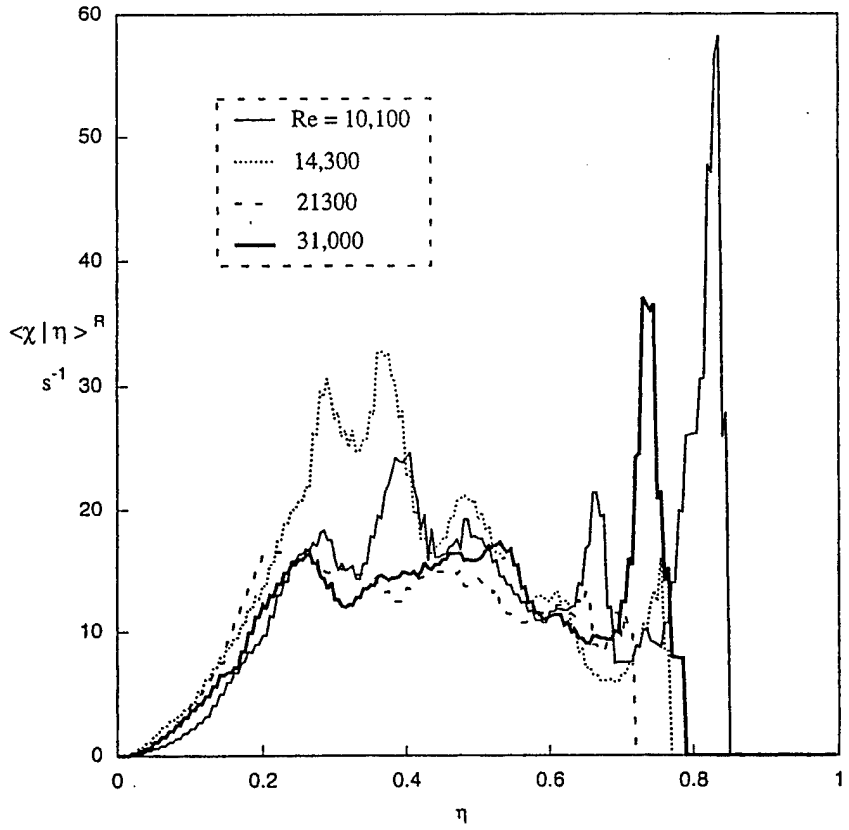

FIGURE 19 CH_4 flames: Scalar dissipation, integrated across the flow, and weighted by the pdf of the mixture fraction (Eq. 3).

weighted by the mixture fraction pdf, is an important quantity. This integral has been computed for the CH_4 flames, and is shown in Figure 19 for the full range of Reynolds numbers. Once again the lack of increase in general magnitude with jet velocity is unexpected and may be due to lack of similarity arising from the significant co-flow. The peaks at high mixture fraction probably arise from low number statistics. The shape at low mixture fraction is noteworthy – an almost parabolic rise is indicated. It is possible to obtain this weighted average of the scalar dissipation by integrating the pdf transport equation. Measurements of the axial velocity component are needed, however, but are not available at this time. This could give a useful check on the measurements, as measurements of pdfs and mean velocity are not sensitive to the degree of resolution of the fine scales, as is needed for direct measurement of the scalar dissipation.

4. CONCLUDING REMARKS

The results demonstrate the viability of the two-scalar method as applied to hydrogen and air-diluted methane diffusion flames. The high-energy intracavity design, combined with contour aligned signal smoothing and a spatial resolution of two to four times the Kolmogorov scale, permits 2D scalar dissipation imaging to be performed with less than 15 percent error due to noise and limited spatial resolution. The good agreement with point measurements by others appears to justify the assumption of one-step chemistry.

The probability density of scalar dissipation, $p(\ln\chi)$, differs from that in isothermal flows. This appears to be an effect associated with combustion, which in this moderate Reynolds number flame reduces the local turbulence Reynolds number and increases the integral length scale around stoichiometric. More comprehensive measurements will be needed to resolve this issue.

The finding that the scalar dissipation does not increase with jet velocity is an unexpected result that must be treated with caution. It is unlikely that it arises from insufficient resolution as the measurements are too well resolved to give so significant an error. It is more likely that the result is due to lack of self similarity in the flow and the greater spread of the jet at high velocity.

Measurements of scalar dissipation conditional on the mixture fraction show behaviour which is inconsistent with the assumption of statistical independence that is sometimes assumed. In the outer part of the flow the

conditional scalar dissipation increases strongly with mixture fraction at low values of mixture fraction and this is consistent with the strongly positive correlation found between the fluctuations in dissipation and mixture fraction. Near the centreline the correlation is not strong but there is a significant nonlinear interdependence of χ and ξ. Results are also presented for the weighted integrals of the conditional dissipation across the flow as are needed by the conditional moment closure method.

Acknowledgements

This work was supported in part by the Australian Research Council and the US Air Force Office of Scientific Research under grant no. AFOSR-91-0150.

References

Barlow, R. S. and Carter, C. D. (1994) Raman/Rayleigh/LIF measurements of nitric oxide formation in turbulent hydrogen jet flames, *Combust. Flame*, **97**, 261–280.

Bilger, R. W. (1991) Conditional moment methods for turbulent reacting flow using Crocco variable conditions, Charles Kolling Research Laboratory TN **F-99**, Department of Mechanical Engineering, The University of Sydney.

Bilger, R. W. (1993a) Scalars and their dissipation in turbulent reactive flows: an overview of measurement needs and capabilities. Paper 59, Western States Section, The Combustion Institute.

Bilger, R. W. (1993b) Conditional moment closure for turbulent reacting flow, *Phys. Fluids A*, **5**, 436–444.

Bilger, R. W. (1993c) *In Experimental Methods in Combustion Flows* (A.M.K.P. Taylor, ed.), Academic Press, pp. 1–51.

Drake, M. C., Pitz, R. W. and Lapp, M. (1984) Laser measurements on nonpremixed hydrogen-air flames for assessment of turbulent combustion models, paper 84-0544, AIAA 22nd Aerospace Sciences Meeting, Reno Nevada; *AIAA J.*, **24**, 905 (1986).

Frank, J. H., Lyons, K. M., Marran, D. F., Long, M. B., Stårner, S. H. and Bilger, R. W. (1995) Mixture fraction imaging in turbulent nonpremixed hydrocarbon flames, *Twenty-fifth Symposium (International) on Combustion*, The Combustion Institute, Pittsburgh PA, pp. 1159–1166.

Jayesh, and Warhaft, Z. (1992) Probability distribution, conditional dissipation and transport of passive temperature fluctuations in grid-generated turbulence, *Phys. Fluids A*, **4**, 2292–2307.

Kailasnath, P., Sreenivasan, K. R. and Saylor, J. R. (1993) Conditional scalar dissipation rates in turbulent wakes, jets, and boundary layers, *Phys. Fluids A*, **5**, 3207–3215.

Kelman, J. B., Masri, A. R., Stårner, S. H. and Bilger, R. W. (1995) Wide field conserved scalar imaging in turbulent diffusion flames, *Twenty-fifth Symposium (International) on Combustion*, The Combustion Institute, Pittsburgh PA, pp. 1141–1147.

Kelman, J. B. and Masri, A. R. (1996) Reaction zone structure and scalar dissipation rates in turbulent diffusion flames, *Comb. Sci. Technol.* (submitted).

Klimenko, A. Y. (1990) Multicomponent diffusion of various admixtures in turbulent flow, *Fluid Dynamics*, **25**, 327–334.

Klimenko, A. Y., Bilger, R. W. and Roomina, M. R. (1995) Some pdf integrals for self-similar turbulent flows, *Combust. Sci. and Tech.*, **107**, 403–410.

Marran, D. F., Frank, J. H., Long, M. B., Stårner, S. H. and Bilger, R. W. (1995) An intracavity technique for improved Raman/Rayleigh imaging in flames, *Optics Letters*, **20**, 791–793.

Muss, J. A., Dibble, R. W. and Talbot, L. (1994) A helium-hydrogen mixture for the measurement of mixture fraction and scalar gradient in non-premixed reacting flows, Paper 612, 32nd AIAA Meeting, Jan 10–13, Reno, NV.

Namazian, M., Schefer, R. W. and Kelly, J. (1988) Scalar dissipation measurements in the developing region of a jet, *Combust. Flame*, **74**, 147–160.

Stårner, S. H., Bilger, R. W., Dibble, R. W. and Barlow, R. S. (1990) Piloted diffusion flames of diluted methane near extinction: mean structure from Raman/Rayleigh/fluorescence measurements, *Comb. Sci. Tech.*, **70**, 111–133.

Stårner, S. H., Bilger, R. W., Dibble, R. W. and Barlow, R. S. (1992) Measurements of conserved scalars in turbulent diffusion flames, *Comb. Sci. Tech.*, **86**, 223–236.

Stårner, S. H., Bilger, R. W., Lyons, K. M., Marran, D. F. and Long, M. B. (1993) Planar mixture fraction measurements in turbulent diffusion flames by a joint Rayleigh and fuel LIF method. Proc. of the 14th International Colloquium on the Dynamics of Explosions and Reactive Systems, Coimbra, Portugal.

Stårner, S. H., Bilger, R. W., Lyons, K. M., Frank, J. H. and Long, M. B. (1994a) Conserved scalar measurements in turbulent diffusion flames by a Raman and Rayleigh ribbon imaging method, *Combust. Flame*, **99**, 347–354.

Stårner, S. H., Kelman, J. B., Masri, A. R. and Bilger, R. W. (1994b) Multi-species measurements and mixture fraction imaging in turbulent diffusion flames, *Experimental Thermal and Fluid Science*, **9**, 119–124.

Stårner, S. H., Bilger, R. W. and Long, M. B. (1995) A method for contour-aligned smoothing of joint 2D scalar images in turbulent flames, *Comb. Sci. Tech.*, **107**, 195–203.

Tennekes, H. and Lumley, J. L. (1973) *A first course in turbulence*, The MIT Press.